212
9-27-79

Hr. 96

ORNL-5565

MASTER

Analysis of Creep-Rupture Data for Reference Heat of Type 304 Stainless Steel (25-mm Plate)

R. W. Swindeman

OAK RIDGE NATIONAL LABORATORY

OPERATED BY UNION CARBIDE CORPORATION · FOR THE DEPARTMENT OF ENERGY

ORNL-5565
Distribution
Category UC-79b, -h, -k

Contract No. W-7405-eng-26

METALS AND CERAMICS DIVISION

ANALYSIS OF CREEP-RUPTURE DATA FOR REFERENCE HEAT OF TYPE 304 STAINLESS STEEL (25-mm PLATE)

R. W. Swindeman

Date Published: September 1979

NOTICE This document contains information of a preliminary nature. It is subject to revision or correction and therefore does not represent a final report.

OAK RIDGE NATIONAL LABORATORY
Oak Ridge, Tennessee 37830
operated by
UNION CARBIDE CORPORATION
for the
DEPARTMENT OF ENERGY

CONTENTS

ANALYSIS OF CREEP-RUPTURE DATA FOR REFERENCE HEAT OF TYPE 304 STAINLESS STEEL (25-mm PLATE)*

R. W. Swindeman

ABSTRACT

We are reporting creep-rupture data for a reference heat (heat 9T2796) of type 304 stainless steel. Temperatures range from 482 to 871°C (900 to 1600°F), and times range from 0.0036 to 50 Ms (1 to 15,000 h). The data include rupture life, tertiary creep, true rupture strain, and true tertiary creep strain. Correlations are developed for rupture life vs engineering stress, modulus-compensated true stress, and modulus-compensated effective stress. The temperature dependence of the correlations is also examined. The tertiary creep is correlated with the rupture life. The rupture strain is correlated with both the modulus-compensated true stress and the modulus-compensated effective stress. Finally, the true tertiary creep strain is correlated with the rupture strain.

For nearly all correlations the behavior pattern is discontinuous in the temperature region around 566 to 694°C (1050 to 1200°F). At lower temperatures the parameters in the correlations exhibit different stress and temperature dependencies than at higher temperatures. This change in behavior results from the development of the $M_{23}C_6$ carbide on grain boundaries and within the matrix. The carbide tends to promote higher creep strength and lower ductility.

INTRODUCTION

Our work was performed as part of an effort to develop design methods for nuclear components that operate in the creep temperature range.[1] This effort includes two broad areas of research: (1) the development of inelastic analysis methods and (2) the development of design criteria. Our data will lead to the development of design criteria that protect against creep rupture.

---

*Work performed under DOE/RRT AG 10 20 42 4 (OH048), "High Temperature Structural Design."

In his paper on fracture mechanism maps, Ashby[2] lists several of the more important fracture modes and indicates that either a strain-to-fracture or a time-to-fracture criterion can be established as a function of stress and temperature. Traditionally, the first step in defining creep-rupture design criteria has been to develop correlations for rupture life (t_r), tertiary creep life (t_3), rupture strain (e_R), or tertiary creep strain (e_3) as functions of imposed variables such as stress, strain rate, and temperature. Hypothesized failure criteria are verified by comparing predictions with results from variable stress, strain rate, and temperature tests. Next, the generalization of the failure criteria to multiaxial stress states is formulated. Often the validity is examined by comparing this generalization with experimental data from multiaxial tests. Ultimately, the failure criteria are shown to be valid for structures that exhibit multiaxial stress gradients that vary according to complex histories. Very few experimental programs are carried this far.

We present data from constant-stress creep-rupture tests on a single heat of type 304 stainless steel (heat 9T2796). The data are used to develop correlations of strain to fracture or time to fracture correlations with stress, strain rate, and temperature. We also present a preliminary metallurgical evaluation as well as a tentative failure mode map. In a subsequent report we will extend correlations to include constant strain rate tensile tests and variable stress and temperature creep-rupture tests.

MATERIAL AND DATA SOURCES

The reference heat of type 304 stainless steel (heat 9T2796) was available in 19 different product forms including plate, bar, piping, formed heads, and a forged billet. Characterization data, including stress-rupture data to 3.6 Ms (1000 h), were collected on many of the products and have been reported by McCoy and Waddell[3] and Swindeman et al.[4] Here we emphasize the behavior of the 25-mm (1-in.) plate. Data are provided in Appendix A. Data for other products have been reported by McCoy[5] (51-mm plate), Sikka[6] (51-mm plate), Schultz and Leyda[7] (16-mm bar), Zamrik[8] (25-mm bar), Herrod and Manjoine[9] (25-mm bar), Natesan and Chopra[10] (16-mm plate), and Voorhees[11] (51-mm plate). In almost all instances the material was tested in the laboratory reannealed condition: 1800 s (0.5 h) at 1093°C (2000°F) in argon followed by a rapid cool.

The 25-mm plate that was used to produce most of the creep-rupture data reported here had the following vendor ladle analysis in weight percents: C, 0.04; Mn, 1.22; P, 0.028; S, 0.015; Si, 0.48; Cr, 18.6; Ni, 9.7; Mo, 0.32; and Cu, 0.24. The nitrogen content determined by ORNL was 0.031. The grain size ranged from 0.24 to 0.12 mm (ASTM grain size 1 to 3), and the room temperature yield was near 186 MPa (27 ksi).[4]

Specimens were threaded-end bars, 6.3 mm (0.25 in.) in diameter in the test sections. Reduced section lengths for half of the specimens were 57 mm (2 1/4 in.), and the rest were close to 32 mm (1 1/4 in.). The procedures for creep-rupture testing generally conformed to the ASTM recommended practice E 139, and details are provided elsewhere.[12] The reproducibility of the creep-rupture data and the factors affecting it are also discussed elsewhere.[4]

DEFINITIONS AND ANALYSIS METHODS

Although time to rupture, t_R, is fairly well-defined for uniaxially loaded test bars, the other terms in creep-rupture testing are somewhat ambiguous. Hence Fig. 1 defines some of the terms used in this report. This figure schematically shows a classical creep curve for total engineering strain vs time consisting of three stages: primary, secondary, and tertiary. The initial loading strain is plotted vertically from the origin, although the actual strain rates during loading were near 8×10^{-4}/s. The elastic loading strain is shown as e_e and is assumed to be constant throughout the test. The plastic loading strain is shown as e_p and is also assumed to be constant throughout the test. In a few instances plastic strain pulses (rapid strain bursts) were observed in the tertiary creep stage. These strains are not included in e_p since they occurred late in life. The transient strain during the primary stage has an asymptotic value, e_t, and the "linear" strain or "plasticity resource," as termed by Ivanova[13] and Booker et al.,[14] is given by the product $e_s t_R$.

ORNL—DWG 79-10378

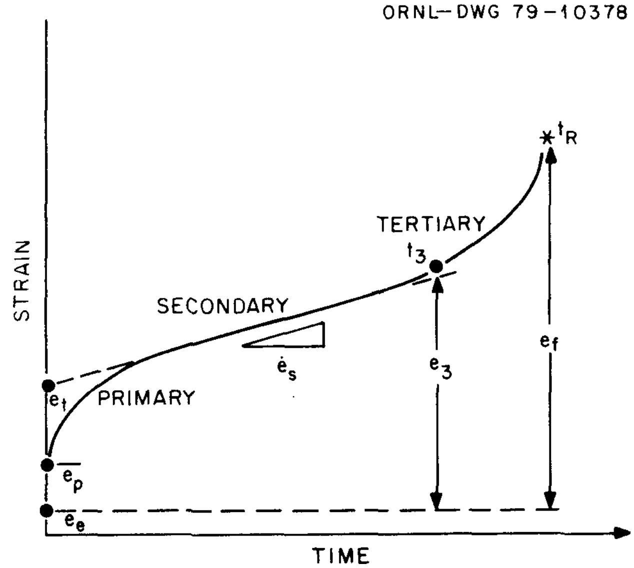

Fig. 1. Definition of Terms Used to Describe Creep-Rupture Data.

The total rupture strain, e_R, includes e_p, e_t, $e_s t_R$, and whatever "strain" is associated with tertiary creep. The time to tertiary, t_3, and the strain to tertiary, e_3, are determined from the creep curve by using the 0.2% strain offset rule of Leyda and Rowe.[15]

As mentioned earlier, data from uniaxial constant stress tests represent only a first step in the development and verification of failure criteria. Ultimately, data must be used in conjunction with some theory generalized to multiaxial stress states and applied to problems that involve fairly small total deformations. Therefore, it is attractive to couch creep-rupture correlations in terms of true stresses and true strains. We attempt to "convert" the engineering stress, S, vs engineering strain, e, into true stress, σ, and true strain, ε. This can be done approximately by multiplying the engineering stress, S, by the term $(1 + e_m)$ to get "true stress" and taking $\ln(1 + e)$ to get "true strain." Here e_m represents the inelastic strain about halfway through the creep test; hence the true stress calculated from ε_m represents the "average" true stress. True stresses were "modulus compensated" by dividing the stress by Young's modulus. Modulus data are provided in Appendix B.

RESULTS

Rupture Life

Before considering the rupture data it is of some value to examine the character of the creep curves at different stresses and temperatures since the deformation behavior could possibly influence the subsequent failure process. In Fig. 2 we have plotted a set of creep curves that terminate at nearly the same rupture life — approximately 2.5 Ms (700 h). Temperatures vary from 482 to 871°C (900 to 1600°F), and stresses vary from 379 to 27.6 MPa (50 to 4 ksi). The plastic loading strain, e_p, is not included. We see that the creep ductility and secondary creep rate diminish with decreasing temperature. Also, the significance of primary creep decreases with decreasing temperature. In fact, the primary creep stage is scarcely noticeable at temperatures below 704°C for this test series. Thus, features of creep deformation, such as the primary creep

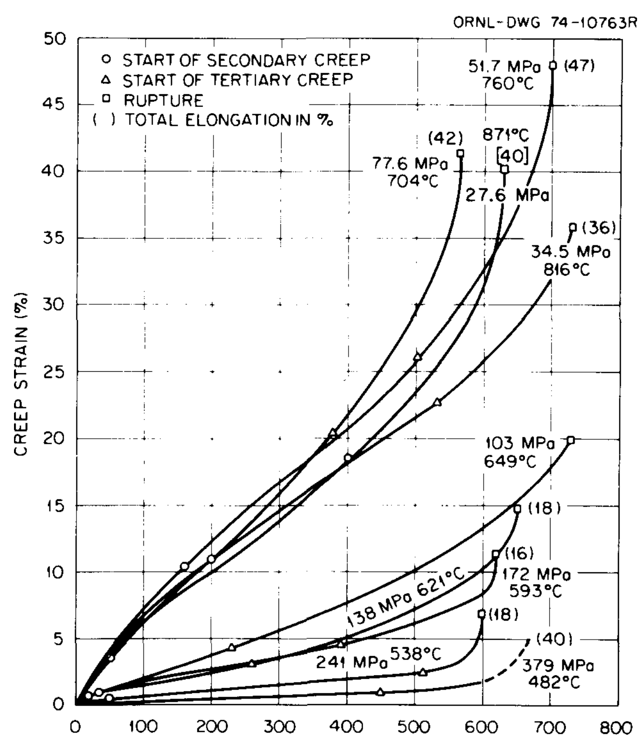

Fig. 2. Influence of Stress and Temperature on the Shape of the Creep Curves for an Approximately 2.5-Ms (700-h) Rupture Life.

strain and secondary creep rate, apparently cannot be used to estimate rupture life without considering a strong temperature related factor.

Changes in the character of creep deformation with stress are shown in Fig. 3 for tests at 593°C. Here we see that for stresses in excess of 138 MPa (20 ksi) the primary creep strain is 1 to 2% compared to the total creep strain of 5 to 9%, while the tertiary creep strain is very prominent. The character of the creep curves changes around 138 MPa (20 ksi). Here the primary creep stage becomes very significant. For example, at 138 MPa (20 ksi), it exceeds 4%. The transition in creep behavior is manifested as a cusp in the log t_R vs log S plot. Data showing this trend are plotted in Fig. 4, which contains information on three product forms: 16-mm bar, 25-mm plate, and 51-mm plate. These products have different grain sizes. The finer grained 16-mm bar appears to have the greatest strength, while the coarser grained 51-mm plate appears to have the lowest strength. The cusp is in the curves for all three products and occurs at the highest stress for the 16-mm bar and at the lowest stress for the 51-mm plate. The cusp is probably related to the precipitation of the $M_{23}C_6$ carbide during the creep process, but how this precipitation affects rupture life is poorly understood.

All the creep-rupture data for the 25-mm product are plotted in Fig. 5. Temperatures range from 482 to 871°C (900 to 1600°F), stresses range from 27.6 to 379 MPa (4 to 55 ksi), and times range from 0.005 to 50 Ms (1.5 to 15,000 h). At most temperatures a cusp is not clearly evident (as it is in Fig. 4); hence, we do not factor the abrupt change in the creep behavior into our rupture correlations.

The straight line through the data for each temperature in Fig. 5 represents the "best fit" of a power law to the data. Thus,

$$t_R = AS^{-n} ,$$

or

$$\ln t_R = a - n \ln S , \tag{1}$$

where A, a, and n are temperature dependent parameters. The parameter values are listed in Table 1 along with statistical data representing

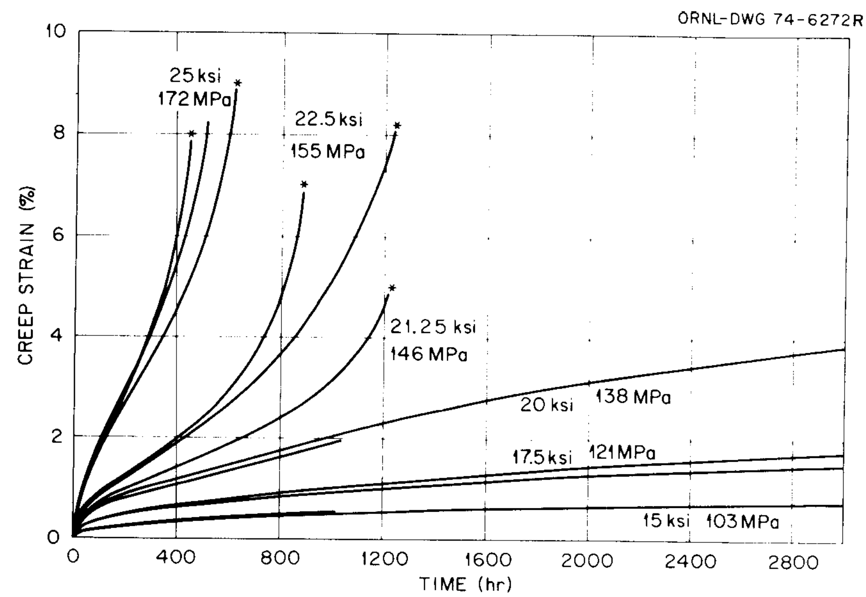

Fig. 3. Influence of Stress on the Shape of Creep Curves at 593°C (1100°F).

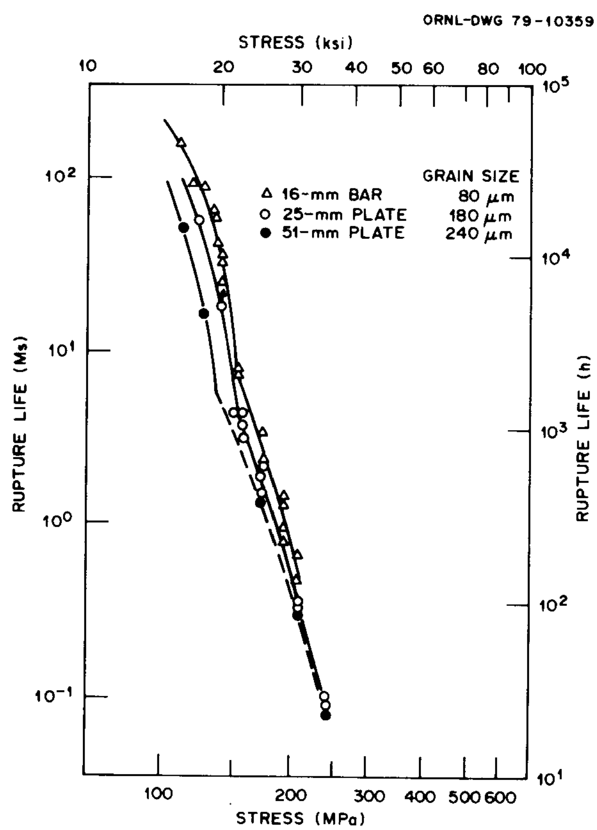

Fig. 4. Influence of Grain Size on the Stress-Rupture Curve at 593°C (1100°F).

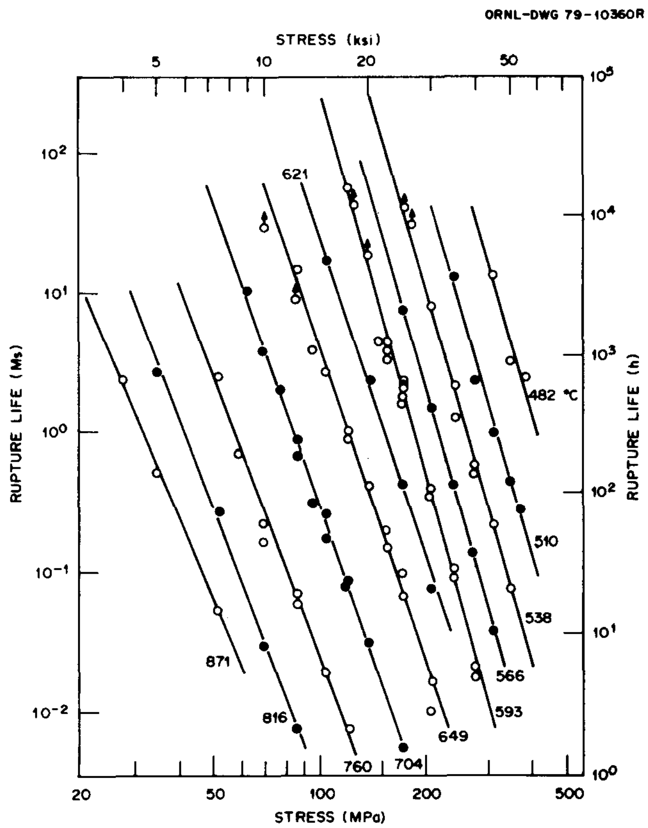

Fig. 5. Rupture Life vs Engineering Stress for Temperatures from 482 to 871°C (900 to 1600°F). Lines represent the fit of a power law to each isothermal data set.

Table 1. Fit of Power Law to Engineering Stress vs Rupture Life[a]

Temperature (°C)	No. Data	n	a	R^2 [b]	SEE[c] (log t_R)
482	3	-8.510	56.85	0.890	0.185
510	5	-8.610	55.14	0.978	0.110
538	7	-8.860	54.84	0.986	0.086
566	5	-8.892	53.46	0.997	0.032
593	19	-9.193	53.58	0.987	0.115
621	4	-7.699	44.28	0.994	0.091
649	12	-7.456	41.31	0.985	0.121
704	12	-7.119	37.11	0.993	0.106
760	9	-6.526	31.94	0.981	0.109
816	4	-6.477	29.65	0.995	0.095
871	3	-5.933	26.06	0.997	0.037

[a] $\ln t_R = a - n \ln S$, with t in h, and S in MPa.

[b] Square of correlation coefficient.

[c] Standard error of estimate in $\log_{10}$ time.

the square of the correlation coefficient (R^2) and the standard error of estimate (SEE). For most temperatures the power law seems to be a fair representation since R^2 values are close to unity, and the standard error of estimate values are not far from the standard deviation replicate tests. For example, the standard deviation for eight replicate tests at 172 MPa (25 ksi) and 593°C (1100°F) is 0.066 log cycle in time.[4] Nevertheless, close inspection of the data for each isothermal reveals some trends that may be significant. We have already discussed the cusp that occurs at 593°C (1100°F), as illustrated in Fig. 4. Another trend is the very high stress data at 482 and 510°C (900 and 950°F). Here, if the points are connected the data seem to "turn upward" with decreasing stress. This will be more evident when we plot true stresses rather than engineering stresses. A third trend is that the data beyond 36 Ms (10,000 h) tend to exhibit longer lives than expected. Since most of the long-time tests were discontinued in the tertiary creep stage, we do not known if power-law extrapolation would be valid at long time. The slopes of the power-law fits in Fig. 5 seem to change with temperature. To show this we have plotted the stress exponent (n) values from Table 1 against the reciprocal of absolute temperature ($1/T$). Behavior is shown in Fig. 6. At temperatures greater than 621°C (1150°F), $|n|$ increases linearly with $1/T$, and n is simply $6900/T$. Between 593 and 482°C (1100 and 900°F) the $|n|$ decreases with increasing $1/T$, while the temperature dependency of n discontinues abruptly between 593 and 621°C. Behavior above 621°C is consistent with expectations if creep rupture is controlled by a stress-dependent activation energy, as assumed by Larson and Miller;[16] however, behavior at lower temperatures does not fit this trend. We believe that the discontinuity between 621 and 593°C (1150 and 1100°F) is real, but the decrease in $|n|$ with decreasing temperature below 593°C (1100°F) is partially caused by the lack of long-time low-stress data and may not be real.

The a values are also plotted in Fig. 6 and show a trend with $1/T$, which in some ways is similar to the temperature dependence of n. However, we assume that a can be represented by the equation:

$$a = \ln A_0 + (Q/RT) \ , \qquad (2)$$

where

A_0 = material constant,

Q = the activation energy for rupture, and

R = the gas constant.

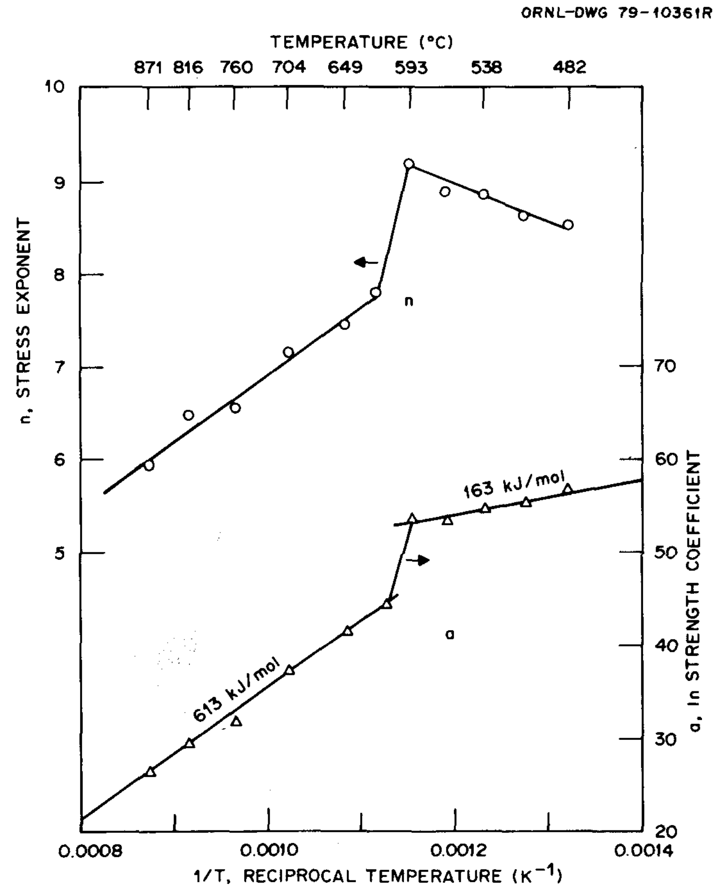

Fig. 6. Stress Exponent, n, and ln Stress Coefficient, a, vs $1/T$, Based on Engineering Stress Data.

The slope of the a vs $1/T$ curves in Fig. 6 relates to the activation energy, and at high temperatures we calculate a value near 613 kJ/mol (147 kcal/mol). Below 593°C (1100°F) we calculate Q to be near 163 kJ/mol (39 kcal/mol). Thus, one model for rupture life in terms of temperature and stress is given in an Orr-Sherby-Dorn[17] expression:

$$t_R = A_0 \exp(Q/RT) S^n \ , \qquad (3)$$

where parameter values depend on temperature and are provided in Table 2. The model is only applicable to uniaxially loaded test bars, which fail by complete separation. This restriction is partly because the stress is engineering stress rather than true stress.

Table 2. Fit of Exponential Equation to the Strength Coefficient[a]

Temperature (°C)	A_0	Q (kJ)	n	R^2
482	1.94×10^{13}	163	-8.50	.911
510	1.94×10^{13}	163	-8.65	.911
538	1.94×10^{13}	163	-8.85	.911
566	1.94×10^{13}	163	-9.00	.911
593	1.94×10^{13}	163	-9.15	.911
621	1.89×10^{-17}	613	-7.75	.995
649	1.89×10^{-17}	613	-7.50	.995
704	1.89×10^{-17}	613	-7.05	.995
760	1.89×10^{-17}	613	-6.65	.995
816	1.89×10^{-17}	613	-6.30	.995
871	1.89×10^{-17}	613	-6.00	.995

[a] $t_R = A_0 \exp(Q/RT)S^n$.

The rupture life is plotted against modulus-compensated "true-stress" data in Fig. 7. Although the general trend of the data is similar to the trend in Fig. 5, the stress sensitivity reflected by the slope of the curves is not as severe when "true stress" is considered. This is especially evident at the lower temperatures where the large plastic loading strain causes more of a stress adjustment at high stresses than at low stresses. As with the engineering-stress data, an effort was made to fit a power law to the stress vs life data. The equation was written:

$$\ln t_R = a' - n' \ln(\sigma/E) , \tag{4}$$

where

a' and n' = temperature dependent material parameters, and

E = Young's modulus.

ORNL-DWG 79-10362

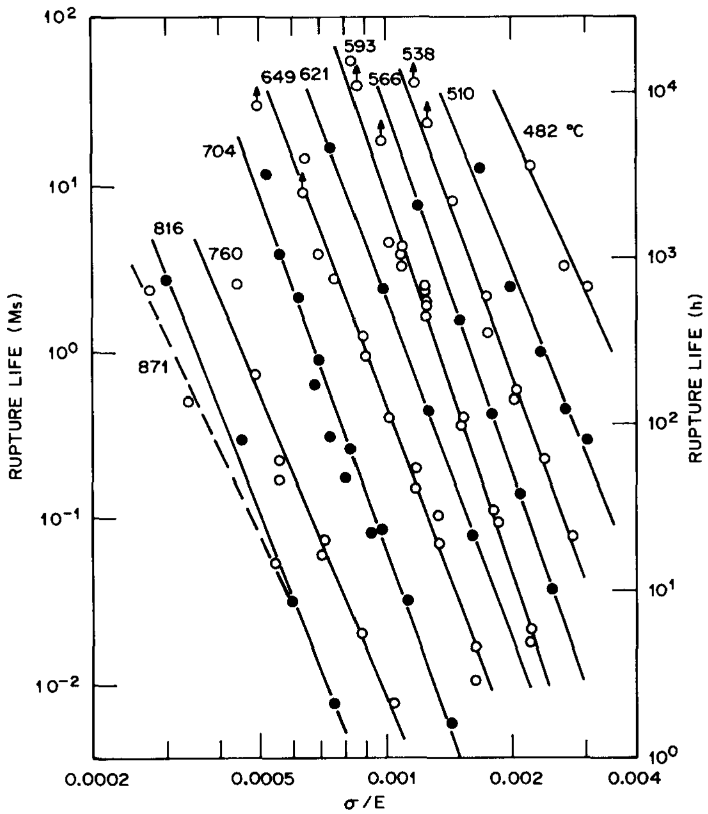

Fig. 7. Rupture Life vs Modulus-Compensated True Stress for Temperatures from 482 to 871°C (900 to 1600°F). Lines represent the fit of a power law to each isothermal data set.

The parameter values are listed in Table 3 along with statistical data (R^2 and SEE). The fit of the power law equation to true-stress data is almost as good as the fit to engineering-stress data; however, there seems to be some important distinctions. First, the n' values for true-stress data generally fall in the range -6 to -8 compared to -6 to 9.15 for n, and behavior changes less abruptly between 593 and 621°C (1100 and 1150°F). Second, the power law clearly underpredicts the life for long-time tests. With regard to the first distinction mentioned above, n' and a' increase with increasing $1/T$, go through a maximum at 593°C, and decrease with increasing $1/T$ at low temperatures. The data at 482 and 510°C (900 and 950°F) are greatly affected by the tests at the highest stresses. When these data were deleted $|n'|$ increased to more than 7. Probably we should assume that $|n'|$ is a constant and is near 7.5 at no greater than

Table 3. Fit of Power Law to Modulus-Compensated True Stress vs Rupture Life[a]

Temperature (°C)	No. Data	n'	a'	R^2 [b]	SEE[c] (log t_R)
482	3	-5.572	-25.91	0.930	0.147
510	5	-6.400	-32.97	0.970	0.140
538	7	-6.981	-38.08	0.984	0.091
566	5	-7.327	-41.58	0.999	0.015
593	19	-7.550	-44.30	0.984	0.117
621	4	-6.843	-40.89	0.999	0.046
649	12	-6.772	-41.88	0.983	0.132
704	12	-7.097	-46.20	0.971	0.165
760	9	-6.237	-42.28	0.969	0.176
816	4	-6.517	-46.11	0.995	0.111
871	3	-5.315	-37.28	0.986	0.079

[a] $\ln t_R = a' + n' \ln(\sigma/E)$, with t in h.

[b] Square of correlation coefficient.

[c] Standard error of estimate in $\log_{10}$ time.

593°C (1100°F). The scatter in n' above 593°C (1100°F) makes it difficult to establish any well-defined trend. This scatter partly results from the influence of the creep ductility on the term needed to adjust the engineering stresses to produce the true-stress data. Nevertheless, $|n'|$ decreases with decreasing $1/T$ (or increasing temperature) and is more-or-less proportional to $1/T$. Assuming this to be true, n' is given by $-6400/T$ at temperatures above 593°C (1100°F).

The a' values plotted in Fig. 8 exhibit considerable scatter also. At temperatures in the range 482 to 593°C (900 to 1100°F), $|a'|$ more-or-less decreases linearly with increasing $1/T$, and we estimate an apparent activation energy near 894 kJ/mol (213 kcal/mol). This activation is much too high to be significant and partly reflects the influence of the temperature variation in n'. Above 593°C (1100°F) a' is relatively constant. This implies that a' is independent of temperature, and hence, the activation energy is nil. Therefore, all the temperature dependency of the rupture life is accommodated by the temperature variation in n'. Although such behavior is inconsistent with the widely held belief that power-law creep is thermally activated, a recent evaluation by Poirier[18]

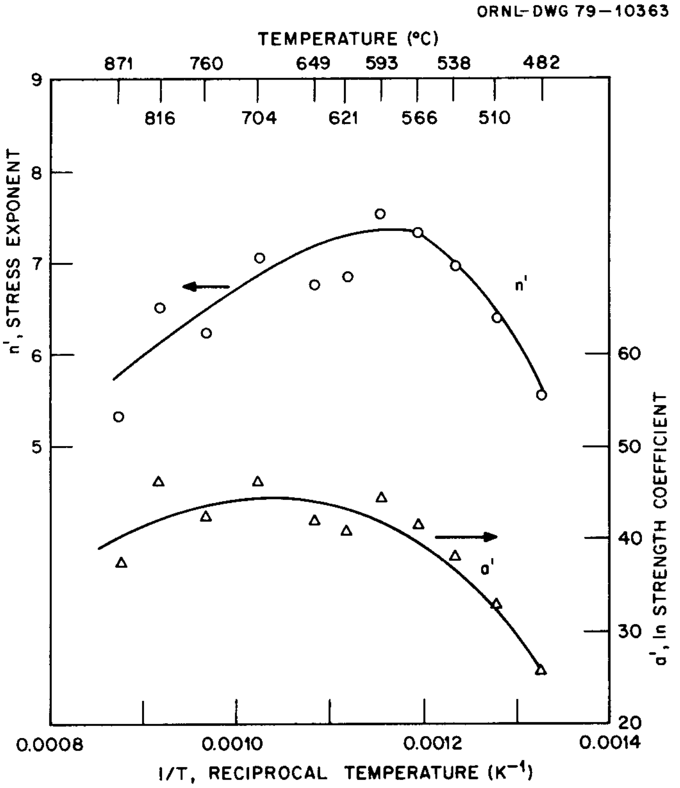

Fig. 8. Stress Exponent, n', and Log Strength Coefficient, a', vs $1/T$. Based on modulus-compensated true-stress data.

indicates that approaches exist that do not require thermal activation energies of the type related to lattice or grain boundary diffusion.

We have analyzed S vs t_R and σ/E vs t_R on the basis of power-law fits to isothermal data. These fits produce analytical expressions that are useful in the range of stresses and times where data exist. The complicated temperature dependence of the parameters in the power laws suggests that interpolation or extrapolation of the power-law equation parameters is risky. It should also be recognized that other analysis procedures produce different trends. For example, in another study we mapped the stress exponent, n', and activation energy, Q, as a function of stress and temperature.[19] This was accomplished by evaluating n' from pairs of data closely spaced on isothermal curves and evaluating Q from pairs of data closely spaced on isostress curves. When the analysis was performed in this way, we found that n' and Q varied slightly with both temperature and stress. At temperatures where a' is relatively insensitive to temperature, the Q determined from isostress evaluation was roughly the same as the activation energy for lattice diffusion. The stress exponent and activation energy maps are in Appendix C.

In another study the whole data set was included in a least squares fit to the Barrett-Ardell-Sherby[20] parameter. The analysis produced a single n' and a single Q that represent all stresses and temperatures. The stress exponent was near -7.0, and the activation energy was near 300 kJ/mol (76 kcal/mol). The data are plotted according to the Barrett-Ardell-Sherby parameter in Appendix A and support the following equation:

$$t_R = A_0' \exp(Q/RT)(\sigma/E)^{-7} \ . \tag{5}$$

As mentioned earlier, examination of the data plotted in Fig. 7 reveals that the power law generally underpredicts the rupture lives for times beyond 1 Ms (2700 h). To capture the long-time rupture behavior, curves that break upward with increasing times must be produced. One way to accomplish this is to introduce the concept of an "effective stress," σ^*/E, which represents the difference between the applied stress, σ/E, and an internal stress or friction stress, σ_0/E. The "friction stress" concept has been used quite successfully by Wilshire and coworkers.[21,22] For isothermal conditions we have:

$$t_R = A''(\sigma^*/E)^{n''} = A''[(\sigma/E) - (\sigma_0/E)]^{n''} \ , \tag{6}$$

where σ_0/E represents a friction stress that may vary with temperature and applied stress. Generally n'' is taken to be near -4; hence, if we take the negative fourth root of Eq. (6), the plot of $t_R^{-0.25}$ vs σ/E should be linear. Figure 9 shows the data trend; the lines represent a least squares fit to the data. Except for a few high-stress data at 566, 593, and 649°C (1100, 1050, and 1200°F), the fit seems to be satisfactory. The equation parameters are provided in Table 4 and plotted in Fig. 10. The σ_0/E data exhibit a fairly complicated pattern. Values are very low at high temperature and increase to a peak at 538°C (1000°F). At lower

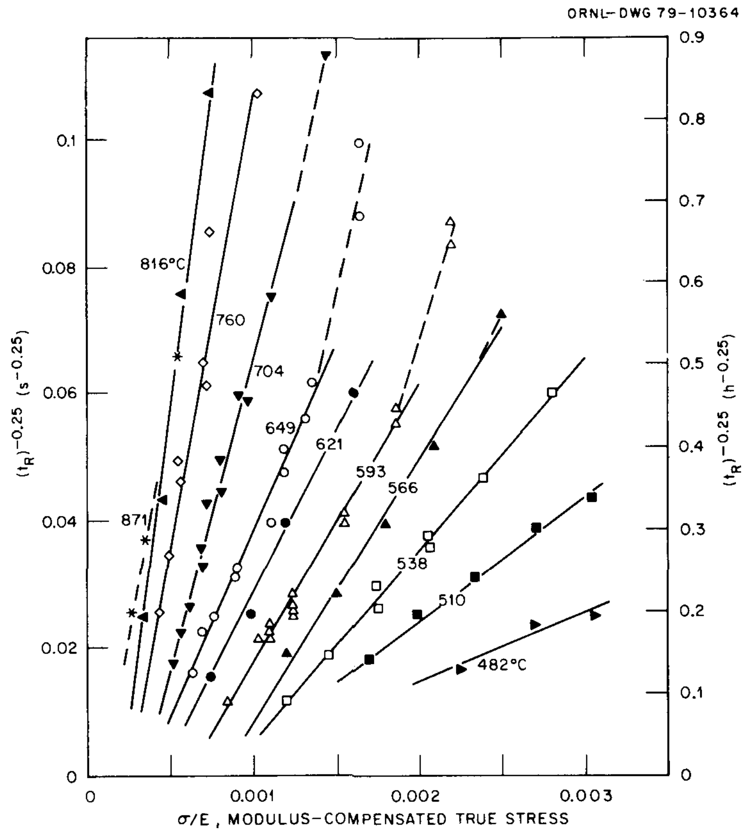

Fig. 9. Fourth Root of Reciprocal Rupture Life vs Modulus-Compensated True Stress.

Table 4. Fit of Effective Stress Representation to Rupture Life[a]

Temperature (°C)	No. Data	n''	ln A''	σ_0/E	R^2[b]	SEE[c] (log t_R)
482	3	-4	-17.72	0.64×10^{-3}	0.923	.142
510	5	-4	-20.08	0.76×10^{-3}	0.983	.112
538	7	-4	-21.84	0.84×10^{-3}	0.992	.075
566	5	-4	-23.08	0.80×10^{-3}	0.991	.136
593	17	-4	-23.38	0.62×10^{-3}	0.972	.155
621	4	-4	-23.91	0.46×10^{-3}	0.987	.181
649	10	-4	-24.48	0.35×10^{-3}	0.989	.091
704	12	-4	-26.66	0.35×10^{-3}	0.986	.121
760	9	-4	-27.96	0.25×10^{-3}	0.987	.143
816	4	-4	-29.11	0.19×10^{-3}	0.987	.257
871	3	-4	-28.05	0.088×10^{-3}	0.995	.113

[a] $\ln t_R = \ln A'' + n'' \ln[(\sigma/E) - (\sigma_0/E)]$, with t in h.

[b] Square of correlation coefficient.

[c] Standard error of estimate in $\log_{10}$ time.

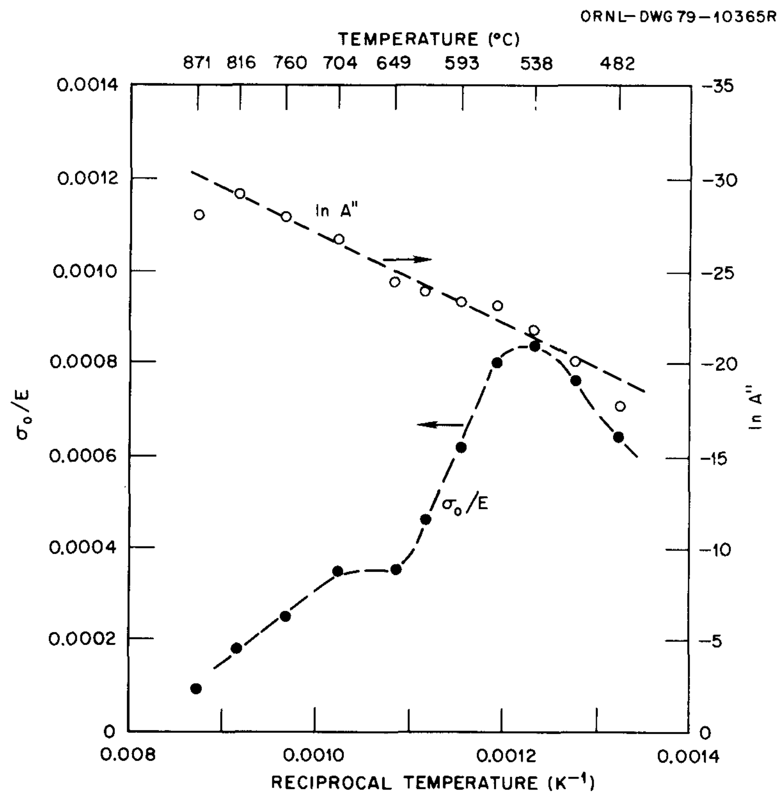

Fig. 10. Friction Stress and Log Strength Coefficient vs $1/T$ Based on Modulus-Compensated Effective Stress Data.

temperatures σ_0/E decreases again. The decrease in σ_0/E at low temperature may reflect the lack of long-time, low-stress data, and fit to the data at 482 and 510°C (900 and 950°F) is not greatly changed if we assume that σ_0/E is constant and close to 0.0008. At high temperature the trend is difficult to model, and more long-time data are needed to establish validity of the visually drawn curve.

The ln A'' values are more-or-less linear with $1/T$, except for data at temperature extremes. If we assume that

$$A'' = A_0 \exp(Q/RT) \ , \qquad (7)$$

then Q is close to 199 kJ/mol (47.6 kcal/mol), and A_0 is near 6.84×10^{-23}. There is sufficient variation in A'' about the fit to permit Q to change smoothly with values ranging from 100 to 300 kJ/mol. Hence, the best fit value of 199 kJ/mol may not have any physical significance. Nevertheless, we can model the data reasonably well by the expression:

$$t_R = 6.84 \times 10^{-23} \exp(199/RT)[(\sigma/E) - (\sigma_0/E)]^{-4} \text{ ,} \tag{8}$$

where σ_0/E data must be determined from Fig. 10.

Although the Wilshire approach has the advantage of curving toward high apparent $|n'|$ values as σ/E approaches σ_0/E, it also requires that σ_0/E decrease sooner or later. Otherwise, the rupture life at some finite stress would be infinite. Data are not available to determine the stress at which σ_0/E should decrease with decreasing stress, except in a few instances. One set of data at 593°C (1100°F) is shown in Fig. 4. Here the trend for the 16-mm bar product exhibits very high apparent $|n|$ values around 138 MPa (20 ksi) and lower $|n|$ values below 138 MPa. We suggest that below 138 MPa we have:

$$(\sigma_0/E) \propto (\sigma/E) \text{ ,}$$

and

$$t_R \propto (\sigma/E)^{-4} \text{ .} \tag{9}$$

In summary, the rupture life can be correlated with the engineering-stress data by means of a power law. The correlation works fairly well in the range from 3600 s to 36 Ms (1 to 10,000 h). The stress exponent and activation energy for creep vary substantially, and it is necessary to divide the correlation into different behavior regimes based on temperature. The rupture life can also be correlated with true-stress data by a power law. Although the stress exponents and activation energies do not vary as widely as engineering stress data, it is still necessary to divide the correlation into different regimes of behavior. There is also a tendency to underpredict the rupture lives at long times. The introduction of friction stress into the stress term and the assumption that the stress exponent is -4 produces a reasonable model for the rupture life in the time range of our interest. However, the temperature dependence of the friction stress is difficult to model, and it is necessary to assume that the friction stress is proportional to the applied stress at low stresses.

Tertiary Creep Life

The simplist method of developing a correlation for the tertiary creep life, t_3, is to relate t_3 to the rupture life, t_R, as was done by Leyda and Rowe[15] in 1969. Thus, if we can decide on a useful model for the rupture life, the tertiary creep correlation follows directly. Plots of t_3 vs t_R data are shown in the next three figures. Figure 11 includes data for 871, 816, 760, and 704°C (1600, 1500, 1400, and 1300°F). The symbols represent the t_3 vs t_R, where t_3 is based on the 0.2% offset strain. When significantly different from t_3, the time when the creep curve noticeably departs from the secondary stage is also indicated by dropping a vertical line from the symbol to the time of departure from the secondary creep stage. Generally, both definitions for tertiary creep produce similar trends. For the four temperatures considered in Fig. 11 the relation between t_3 and t_R is close to linear, and ratio t_3/t_R seems to be in the range 0.5 to 0.7. Data for 649, 621, 593, and 538°C (1200, 1150, 1100, and 1050°F) are plotted in Fig. 12. An unusual trend appears

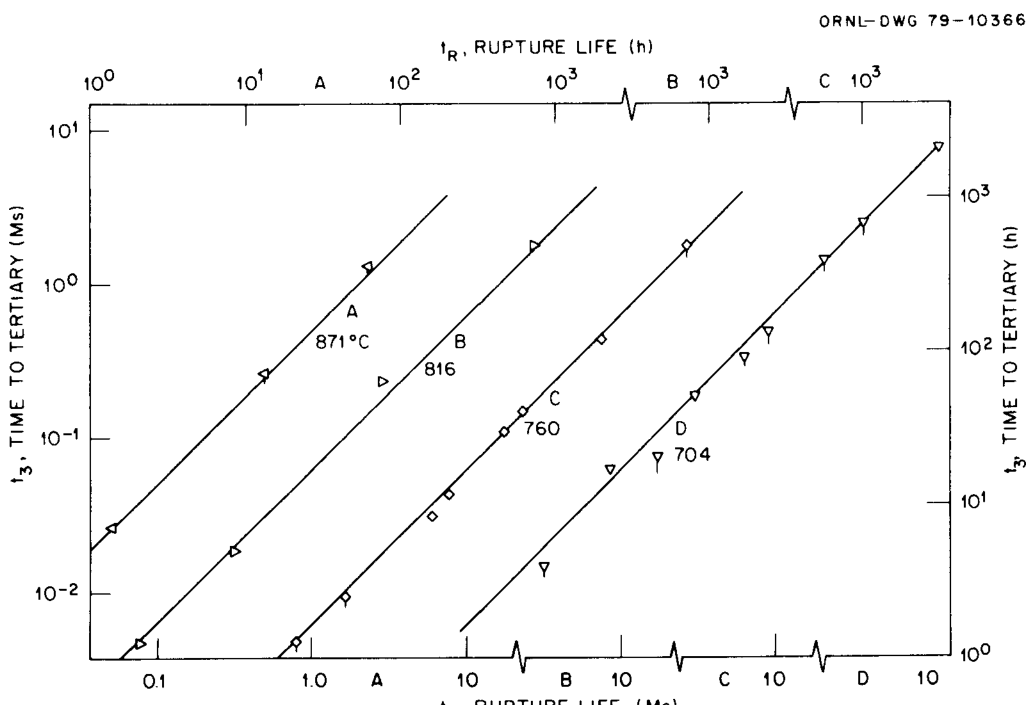

Fig. 11. Tertiary Creep Life, t_3, vs Rupture Life, t_R, at 871, 816, 760, and 704°C (1600, 1500, 1400, and 1300°F).

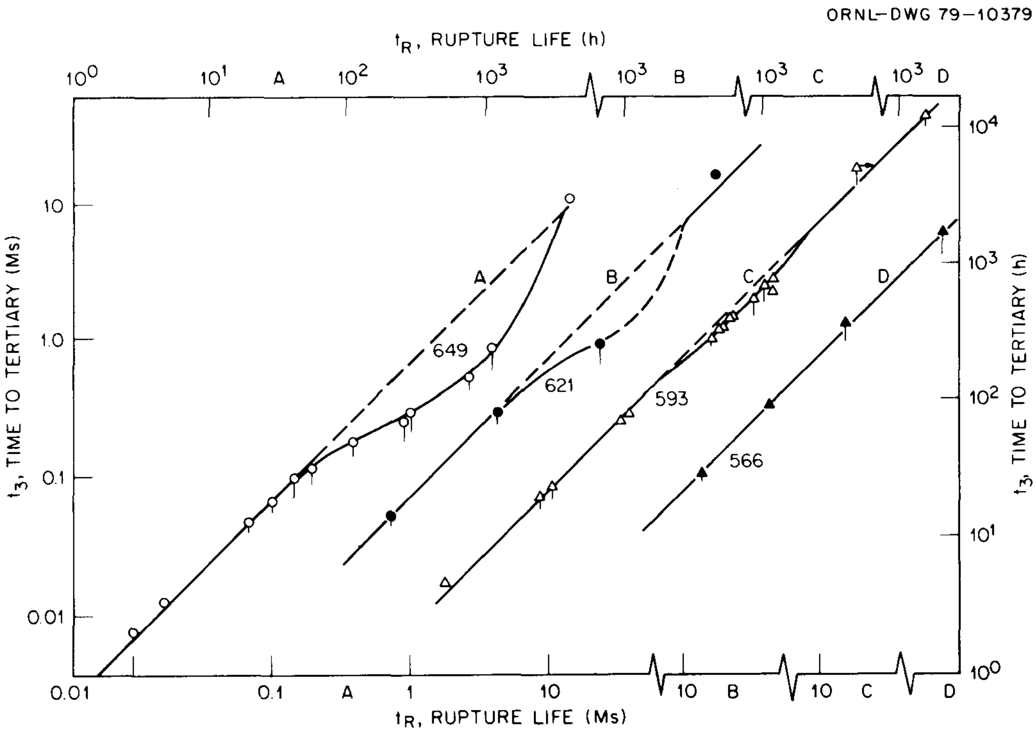

Fig. 12. Tertiary Creep Life, t_3, vs Rupture Life, t_R, at 649, 621, 593, and 566°C (1200, 1150, 1100, and 1050°F).

in the data at 649°C (1200°F). For test data out to approximately 0.18 Ms (50 h) behavior is similar to high-temperature trends, and the ratio t_3/t_R is near 0.7. However, at longer times the ratio decreases significantly to around 0.2 and does not recover to higher values until rupture lives exceed 10 Ms (3600 h). Similar but less dramatic behavior is present at 621°C (1150°F). Here we see departure from the linear trend at times for t_R greater than 0.5 Ms (150 h). Linear behavior between t_3 and t_R is observed at lower temperatures and the ratio t_3/t_R is near 0.75 at 593°C (1100°F) and near 0.8 at 566°C (1050°F). There is some evidence for departure from linearity at 593°C (1100°F) when t_R is in the range 1 to 5 Ms (300 to 1500 h), but perhaps the departure results more from the scatter in the data. Test data for 528, 510, and 482°C (1000, 950, and 900°F) are plotted in Fig. 13. Because of the difficulty in defining the time to tertiary creep at the very high stresses, the data at 510 and 482°C (950 and 900°F) must be regarded as very tenuous. Instead of using the actual data to define t_3/t_R at low temperatures, we suggest that the trend at

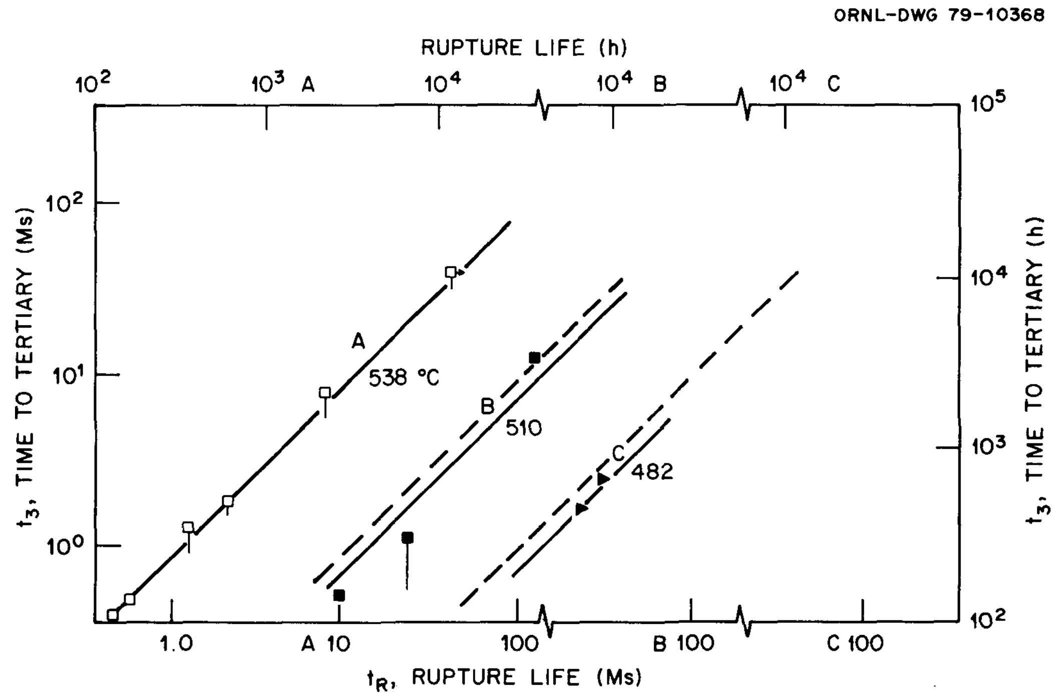

Fig. 13. Tertiary Creep Life, t_3, vs Rupture Life, t_R, at 538, 510, and 482°C (1000, 950, and 900°F).

higher temperatures be extrapolated to lower temperatures. A linear extrapolation of the t_3/t_R ratios in the temperature range 704 to 538°C (1300 to 1000°F) indicates that t_3/t_R should be near 0.87 at 510°C (950°F) and 0.91 at 482°C (900°F). These ratios are plotted as dashed lines in Fig. 13. If these trends are valid then we can expect that t_3/t_R will be close to unity at 427°C (800°F).

Except for the deviation from linearity at 649 and 621°C (1200 and 1150°F), we suggest that the tertiary creep life, t_3, can be correlated to the rupture life, t_R, by using the ratio values plotted in Fig. 14 and tabulated in Table 5.

Rupture Strain

The creep-rupture strain can be represented by either the elongation or the reduction of area. Either of these quantities can be described as engineering strain or true strain. We will emphasize the true stain based on reduction of area measurements, ε_R. Although there is considerable interest in correlating rupture strains with strain rates,[23] we believe

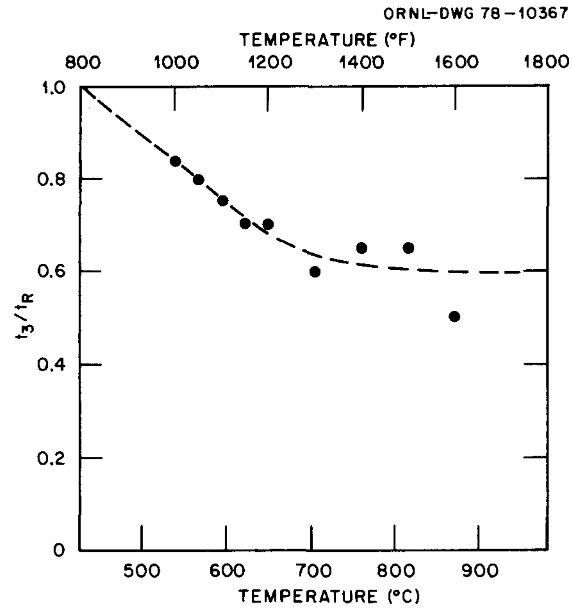

Fig. 14. Ratio t_3/t_R vs Temperature.

Table 5. Ratio of Tertiary Life to Rupture Life

Temperature (°C)	t_3/t_R	
	Experimental	Smoothed
482		0.92
510		0.88
538	0.84	0.84
566	0.80	0.80
593	0.75	0.76
621	0.70	0.72
649	0.70	0.68
704	0.60	0.64
760	0.65	0.61
816	0.65	0.60
871	0.50	0.60

that correlating the rupture strain with the independent variables of stress and temperature is more meaningful. Here we focus on true stress rather than engineering stress and again resort to the modulus-compensated stress (σ/E). However, we must choose how to define σ/E. Should σ/E be based on an "average" stress throughout the test or on the final rupture stress? For consistency with the rupture-life correlation, we elect to use the "true stress" about halfway through the test. Thus, the stress will be more representative of the stress at tertiary creep than at actual rupture.

Plots of ε_R vs σ/E are provided in Fig. 15 for temperatures in the range 482 to 871°C (900 to 1600°F). Data obtained from tensile tests are also included to define the trend over a broader stress range. Even so, the pattern that emerges is not very clear. At temperatures in the range 482 to 593°C (800 to 1100°F), the true rupture strain increases more-or-less linearly for σ/E values up to 0.002 and in some instances nearly 0.004. Eventually, the ε_R data sweep upward almost exponentially to values exceeding 100%. This upward sweep occurs at stresses typical of the true ultimate strength for high-strain-rate tensile tests. No well-defined effect of temperature appears at lower stress levels. Thus, over a limited range of stresses, we can represent the effect of σ/E on ε_R by the simple relation:

$$\varepsilon_R = 12{,}500\ \sigma/E\ . \tag{10}$$

The dashed line plotted in Fig. 15a through 15e represents Eq. (10), and we see that it is a conservative estimate of ε_R for stresses σ/E to at least 0.002. The behavior pattern is different for temperatures above 593°C (1100°F). In Fig. 15f through 15i, data for temperatures in the range 621 to 760°C (1150 to 1400°F) are plotted. At intermediate stresses the fracture strains are fairly high and increase gradually with stress. There is substantial scatter in the data, making it difficult to arrive at an analytical representation. As at lower temperatures the ε_R data exhibit a sharp upward sweep at high σ/E values. By ignoring this high-stress behavior, a possible representation that would capture the trend at low and intermediate σ/E could be based on the exponential form:

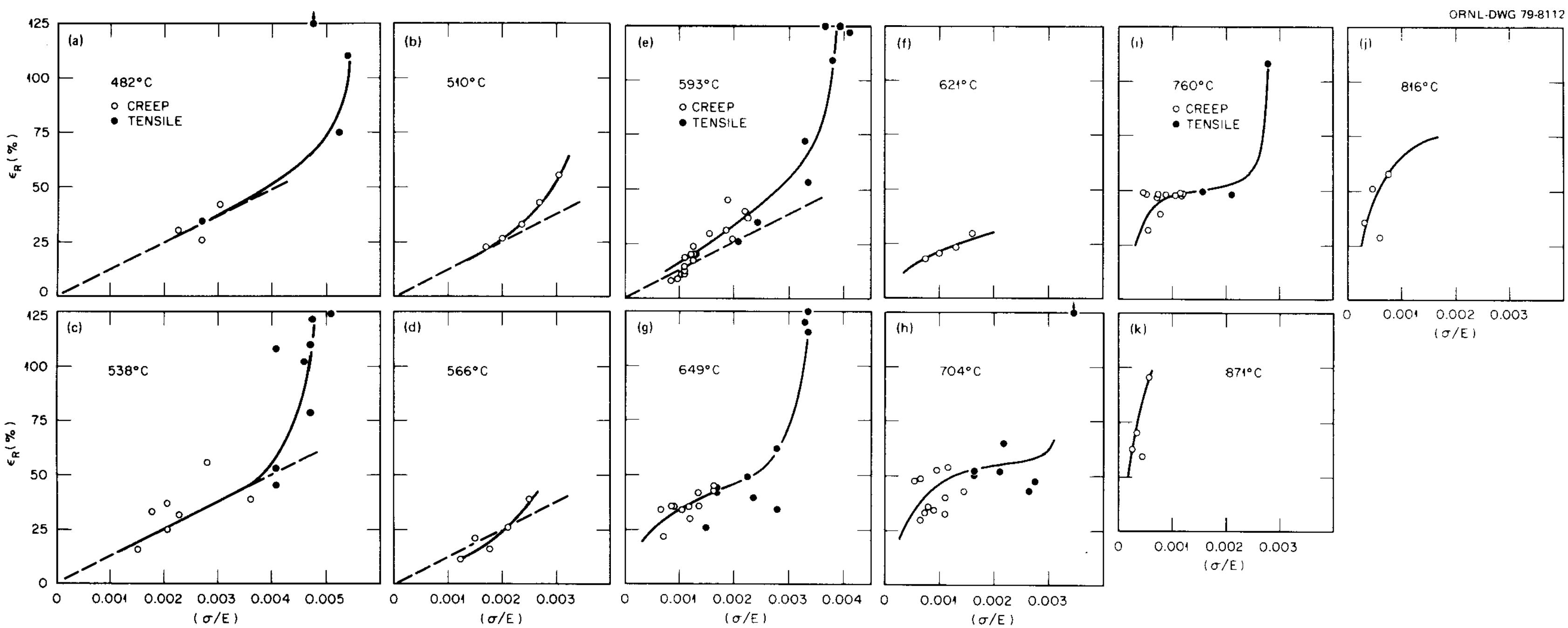

Fig. 15. True Rupture Strain, ε_R, vs Modulus-Compensated True Stress for Temperatures from 871 to 482°C (1600 to 900°F).

$$\varepsilon_R = K[1 - \exp(-\gamma\ \sigma/E)] \ . \tag{11}$$

Here K would represent a rupture ductility that is approached at a rate governed by the value of γ. When the stress is near zero the slope of the ε_R vs σ/E curve is approximately constant and has the value $K\gamma$. At temperatures below 621°C (1150°F) $K\gamma$ does not vary with temperature, and hence Eq. (10) can be considered an approximation of Eq. (11) and valid at low σ/E. At temperatures in the range 621 to 760°C (1150 to 1400°F), $K\gamma$, K, and hence γ can be estimated. At temperatures above 760°C (1400°F) we do not have any high stress data, so K cannot be determined (see Fig. 15j and 15k). However, the low-stress data for σ/E in the range 0 to 0.0005 increase almost linearly, and $K\gamma$ can be estimated. Values are provided in Table 6.

Earlier in the report we showed that the rupture life, t_R, could be correlated with an effective stress (σ^*/E) that represented the difference between the applied stress (σ/E) and a friction stress (σ_0/E). It is reasonable to question if any meaningful relationship between ε_R and σ^*/E exists. There is no clear answer to this question. In the case of the rupture life, we can assume that the friction stress, σ^*/E, increases during the initial plastic loading and primary creep stages. Over much of the rupture life, σ^*/E is reasonably constant; hence, actual conditions can be fairly approximated by using an effective stress based on the true stress about halfway through the life. However, when ε_R is correlated with σ^*/E the plastic loading strains and primary creep strains can be significant components of the rupture strain, and we are not sure these components should be included in the correlation. Nevertheless, in Fig. 16 we show data for temperatures in the range 482 to 621°C (900 to 1150°F). Here the data fall more-or-less on lines that go toward zero with decreasing σ^*/E. The value of ε_R might increase with temperature. If so, in the temperature range 482 to 621°C (900 to 1150°F), we can approximate ε_R vs σ^*/E by the expression:

$$\varepsilon_R = b(T)[(\sigma/E) - (\sigma_0/E)] \ , \tag{12}$$

Table 6. Parameter Values Representing True Fracture Strain vs Modulus-Compensated True Stress[a]

Temperature (°C)	$K\gamma$ (%)	K (%)
482	12,500	
510	12,500	
566	12,500	
593	13,000	
621	30,000	
649	60,000	45
704	75,000	55
760	75,000	50
816	100,000	
871	140,000	

[a] $\varepsilon_R = K[1 - \exp(-\gamma\sigma/E)]$.

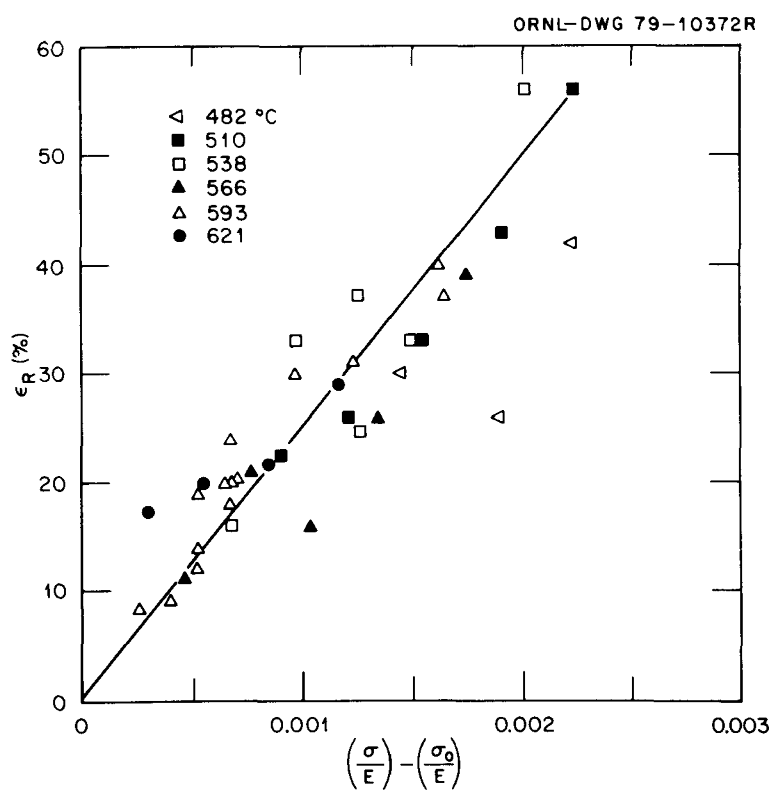

Fig. 16. True Rupture Strain, ε_R, vs Effective Stress, $(\sigma - \sigma_0)/E$, for Temperatures in the Range 482 to 624°C (900 to 1150°F).

where $b(T)$ is some temperature dependent material parameter. From Eq. (6) we have

$$t_R = A_0'' \exp(Q/kT)[(\sigma/E) - (\sigma_0/E)]^{-4} .$$

By eliminating $[(\sigma/E) - (\sigma_0/E)]$ from Eqs. (6) and (8)

$$\varepsilon_R = b(T)[t_R/B_0 \exp(Q/RT)]^{-1/4} , \tag{13}$$

or

$$\varepsilon_R = B(T)/t_R{}^{0.25} . \tag{13a}$$

Tertiary Strain

As established earlier the time to tertiary creep, t_3, can be correlated with the rupture life, t_R, over a broad range of temperatures and times. There are regions at 593, 621, and 649°C (1100, 1150, and 1200°F) where t_3 and t_R follow differing patterns and where correlation is difficult. Similar problems exist in correlating ε_3 and ε_R. However, a well-defined trend exists over much of the data range. In Fig. 17 the ε_3 vs ε_R data are plotted for many temperatures. Generally, ε_3 increased with ε_R at lower temperatures. The slope of the ε_3 vs ε_R trend tends to decrease with increasing ε_R and temperature. For temperatures above 649°C (1200°F) it is difficult to establish any well-defined trend. The results from the fit of a power law through the ε_3 vs ε_R data are in Table 7. For temperatures in the range 482 to 593°C (900 to 1100°F) the exponent in the power law, p, is in the range 0.64 to 0.85, with 0.75 being close to the "average." Thus, we could write:

$$\varepsilon_3 = D(T)\varepsilon_R{}^{0.75} , \tag{14}$$

where $D(T)$ is a temperature dependent material parameter. The R^2 values are in the range 0.79 to 0.99 for temperatures from 510 to 593°C (950 to 1100°F). Above 593°C (1100°F) the p values range from 2.2 to 0.026, and the R^2 values generally indicate a poor fit of the data to the power-law model. Thus, Eq. (14) should not be used above 593°C.

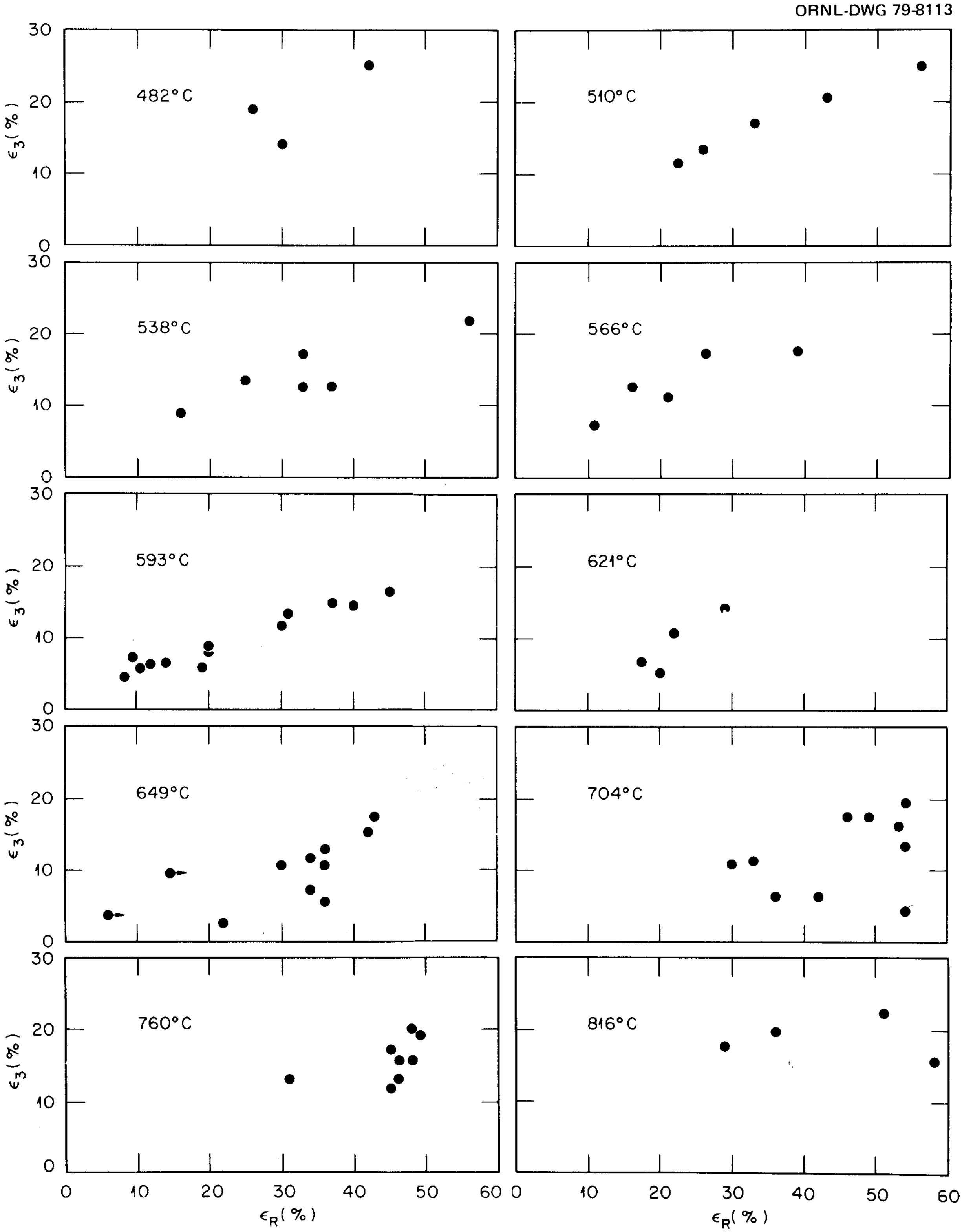

Fig. 17. True Tertiary Strain, ε_3, vs True Rupture Strain, ε_R, for Temperatures in the Range 871 to 482°C (1600 to 900°F).

Table 7. Fit of Power Law to ε_3 vs ε_R Data[a]

Temperature (°C)	No. Data	p	K	R^2[b]
482	3	0.79	1.22	0.46
510	5	0.85	0.83	0.99
538	6	0.64	1.53	0.79
566	5	0.71	1.47	0.83
593	13	0.70	1.08	0.88
621	4	1.74	0.039	0.70
649	10	2.20	0.0037	0.53
704	10	0.57	1.32	0.06
760	8	0.60	1.56	0.22
816	4	0.026	16.7	0.003
871	3	2.14	0.0057	0.99

[a] $\ln \varepsilon_3 = \ln K + p \ln \varepsilon_R$, with ε_R in %.

[b] Square of correlation coefficient.

The straightforward correlation for ε_3 vs ε_R at lower temperatures only signifies the end of the secondary creep stage of tertiary creep strain. However, ε_3 could be an instability of the type that occurs in tensile tests. The experimental justification for this is the fairly good agreement between the uniform strain in tensile tests and the strain to tertiary creep in creep tests. This comparison is shown in Fig. 18, where the ε_3 data from creep tests and ε_μ (the uniform strain) data from tensile tests are plotted against true stress.

Monkman-Grant Correlation

The direct correlation of rupture life with stress and temperature has limited use at very low stresses because of the lack of data. With available techniques low-stress rupture data at high temperatures can be used to predict long-time low-stress rupture data at lower temperatures. These time-temperature parameters are well known.[24] Unfortunately, the strong temperature dependence of the creep-rupture stress exponent, n, in the range 566 to 649°C (1150 to 1200°F) is not consistent with trends expected from the most commonly used time-temperature parameters. An

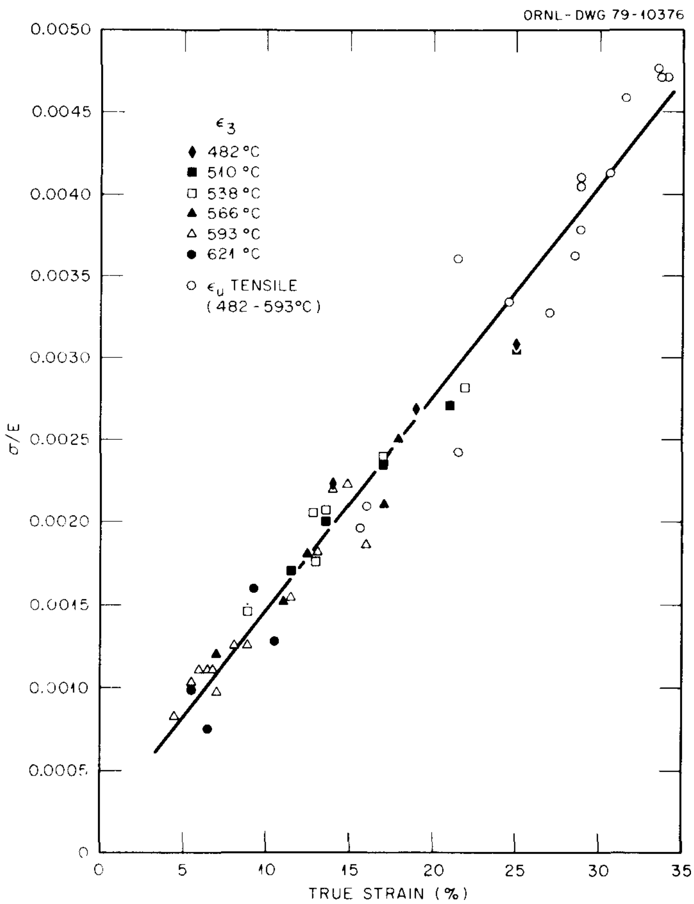

Fig. 18. Comparison of the True Tertiary Strain, ε_3, vs Stress with the True Uniform Strain vs Stress.

alternate correlation method that can be used for isothermal data is based on the relation between rupture life and minimum (or secondary) creep rate. For example, Monkman and Grant[25] have shown that:

$$t_R = c\dot{e}_s^m , \tag{15}$$

where c and m are material parameters. For many materials both c and m are independent of temperature and m is close to -1. If the parameters are independent of stresses as well as temperatures, then the known creep rate at low stresses can be used to estimate the rupture life.

In Fig. 19 we show plots of t_R vs $\dot{e}_s$ data taken from an earlier report.[26] Examination of the data reveals that the slope, m, is near -1.0 at temperatures above 649°C (1200°F) but increases with decreasing

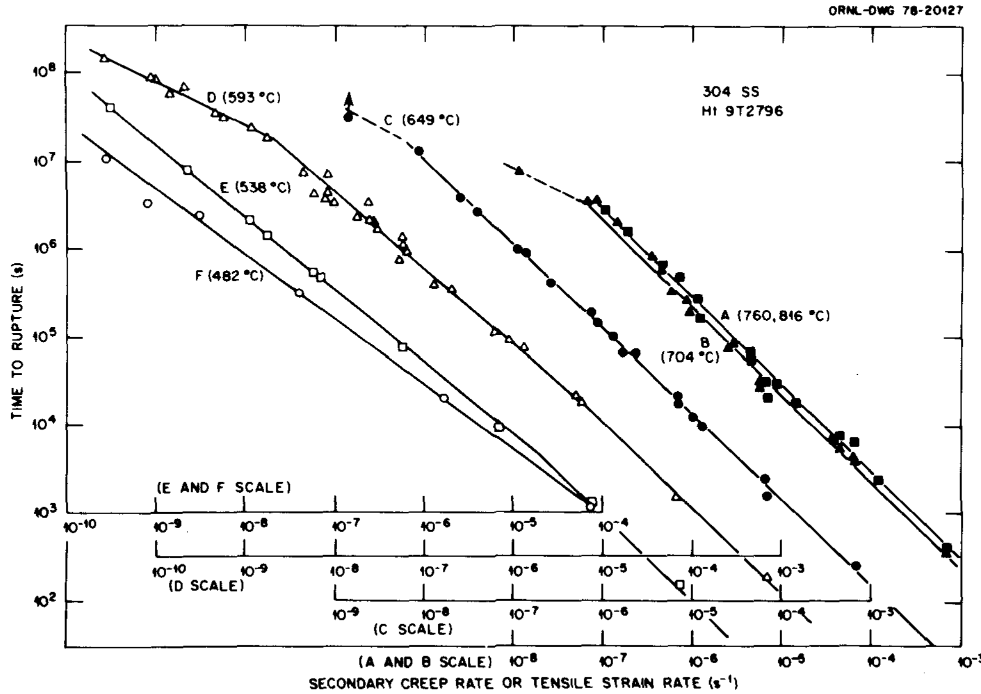

Fig. 19. Effect of Temperature on the Monkman-Grant Correlation Between Rupture Life and Secondary Creep Rate.

temperature. Also, there appears to be a "break" in some of the log t_R vs log $\dot{e}_s$ curves at long times. Furthermore, the position of the curves shifts with temperature. This indicates that c is temperature dependent. Based on these data trends, we conclude that the Monkman-Grant correlation cannot be used for extrapolation for this material, although it could be of value in interpolation.

Failure Modes

The metallurgical evaluation of creep-tested specimens is still in progress; hence, we will limit our discussion to a few qualitative statements. At stresses near the ultimate strength and at 482°C (900°F) the material fails by shearing off, which follows the development of a neck. As stresses are lowered some intergranular wedge-type cracks develop before fracture. The intergranular cracking becomes more prominent as the temperatures are increased and stresses are lowered [See Fig. 20(a)]. At

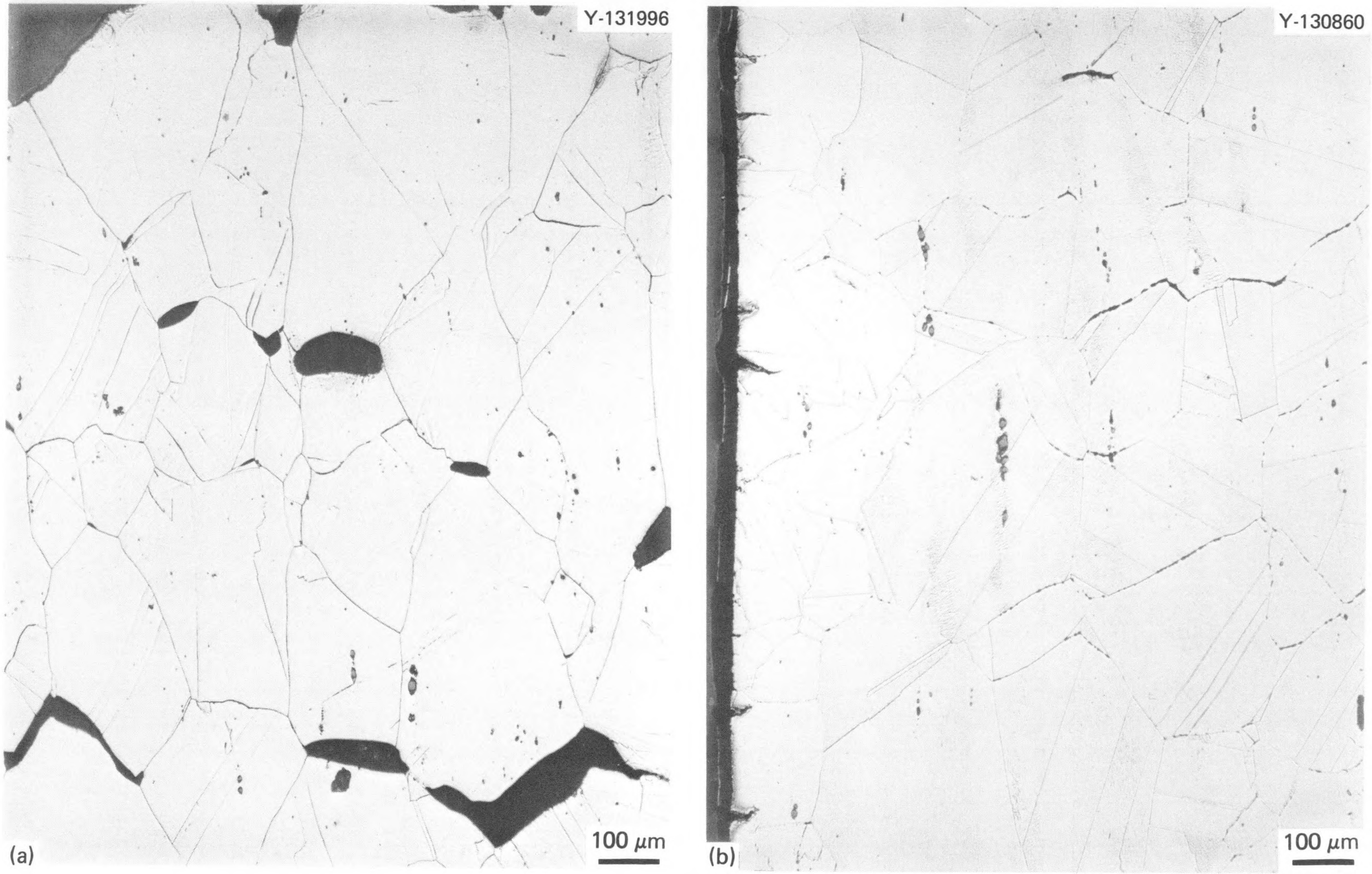

Fig. 20. Ruptured Specimens Showing (a) Wedge Cracking and (b) Microvoid Formation.

593°C (1100°F) wedge-type cracking dominates, but the formation of microvoids on grain boundaries at low stresses is somewhat evident [see Fig. 20(b)]. Above 621°C (1150°F) grain boundary migration is sometimes present, while above 704°C (1300°F) recrystallized material is sometimes present near the fracture surfaces. Although intergranular failures persist at temperatures above 704°C (1300°F) the fracture surface looks ragged as a result of greater grain distortion and environmental attack. Several specimens seemed to fail prematurely. Examination of the specimens revealed that premature failures occurred in abnormally coarse grained regions where the grain size exceeded 200 μm.

For more information about failure modes in austenitic stainless steels, refer to Sikka[6] and Morris and Harries.[26] Our preliminary studies agree qualitatively with their research. Figure 21 is a map for failure modes.

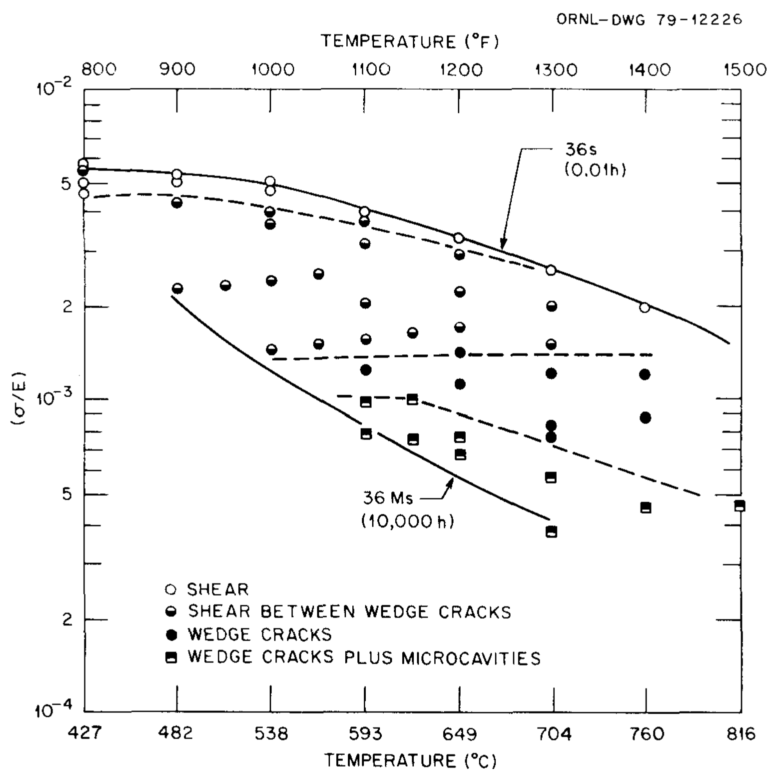

Fig. 21. Failure Mode Map for Type 304 Stainless Steel Heat 9T2796.

DISCUSSION

We have presented several correlations for creep-rupture data and have elected to use a power law for relating the rupture life to the stress at constant temperature. Generally, both the stress exponent and strength coefficient in the power law are temperature dependent and tend to decrease with increasing temperature. The temperature dependence of the strength coefficient seems to follow Arrhenius-type behavior, but the activation energy is not constant throughout the range of temperature and stress that we have examined. The constants also depend on the definition of stress, and we have used S, σ/E, and σ^*/E. We prefer to think in terms of modulus-compensated true stress rather than engineering stress, S, and modulus-compensated effective stress, σ^*/E, rather than σ/E. The modulus-compensated friction stress, σ_0/E, must be calculated from the creep-rupture data to determine σ^*/E. Note that σ_0/E is not necessarily the same as the friction stress studied by Wilshire and coworkers[21,22] or the internal stress studied by Ahlquist and Nix.[27] However, we logically expect the friction stress to change during the course of the creep process. Hence, the modulus-compensated effective stress, σ^*/E, will not be constant.

Étiènne, Dortland, and Zeedijk[28] and Shinoda et al.[29] clearly show that the metallurgical processes that occur during creep on type 304 stainless steel have a significant influence on subsequent rupture processes. Recently, Morris and Harries[26] have shed more light on this same phenomenon for type 316 stainless steel. All these researchers find that the $M_{23}C_6$ carbide that precipitates during creep greatly influences the substructure. Furthermore, the substructure within the matrix controls the deformation rate, and the substructure within and near the grain boundaries controls the grain boundary sliding rate. Since substructural change can be represented by the change in the friction stress, σ_0/E, we feel that the modulus-compensated effective stress, $(\sigma - \sigma_0)/E$, is a better variable to relate to rupture life or to fracture strain than is the modulus-compensated true stress, σ/E, or the engineering stress, S.

Although we have not completed our metallurgical study of creep ruptured specimens, we know a great deal about the substructure and deformation processes that lead to rupture. These are discussed below with the aid of the next four figures.

At our lowest temperature, 482°C (900°F), rupture results from creep-induced plastic instability. The plastic loading strain, e_p, is very large for tests with rupture lives less than 36 Ms (10,000 h). These strains introduce high dislocation densities, which are stored in loose cellular configurations (Fig. 22). The friction stress is very high, and the creep process is likely dominated by either dynamic or thermal recovery within the cellular substructure. This is comparable to stage IV hardening in a tensile test. With $M_{23}C_6$ carbide absent grain boundaries can slide. Little capability for matrix hardening combined with relative ease of grain boundary sliding produces high stress concentrations at grain boundary triple points. This leads to wedge cracking. The deformation leads to a loss in load-bearing area and to eventual rupture by a shearing off between grain surfaces that contain wedge cracks (see curve A in Fig. 23). However, a creep test now in progress at 482°C and at an engineering stress of 248 MPa (36 ksi) exhibits a sigmoidal rather than tertiary creep curve (see curve B in Fig. 23). We suspect that the lower stress level: (1) produces less initial matrix strain, (2) reduces the rate of grain boundary sliding, and (3) allows time for additional hardening by the precipitation of $M_{23}C_6$ carbide on grain boundary dislocations and matrix cell walls.

The behavior at 510°C (950°F) resembles that at 482°C (900°F), except that there is less shearing off and more grain boundary wedge cracking at 510°C (950°F) than at 482°C (900°F). Again, the testing times are fairly short relative to the time needed to produce a stable metallurgical structure. High loading strains produce a cellular substructure, and the resulting creep curves for engineering stresses in excess of 241 MPa (35 ksi) are tertiary or sigmoidal (see curve B in Fig. 23). One creep test at an engineering stress of 172 MPa (25 ksi) is in progress and has exceeded 72 Ms (20,000 h). The initial strain is too low to form cells, and the curve exhibits substantial primary

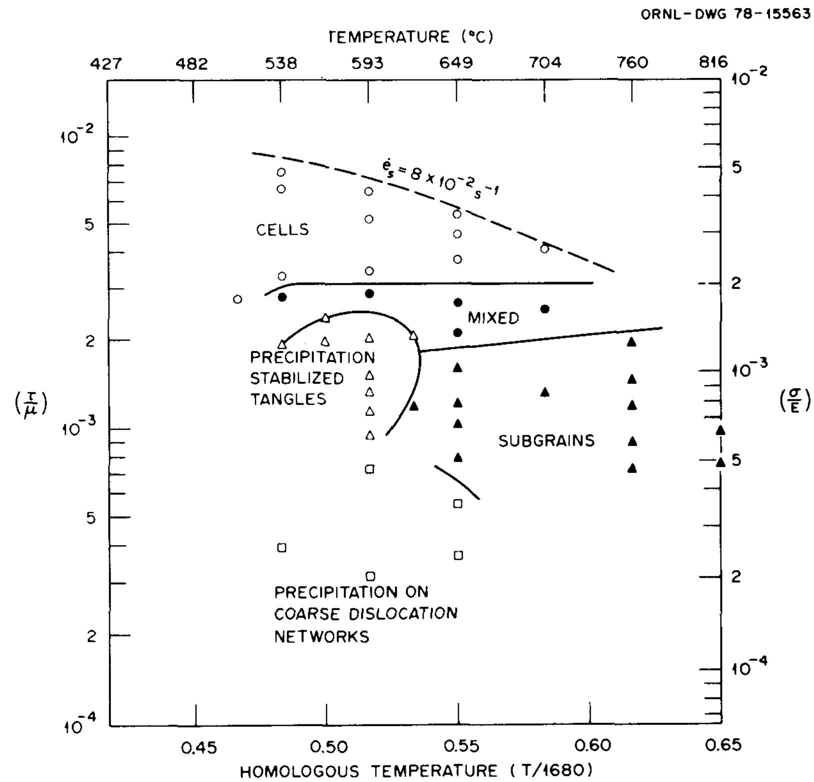

Fig. 22. Substructure Map for Type 304 Stainless Steel Heat 9T2796.

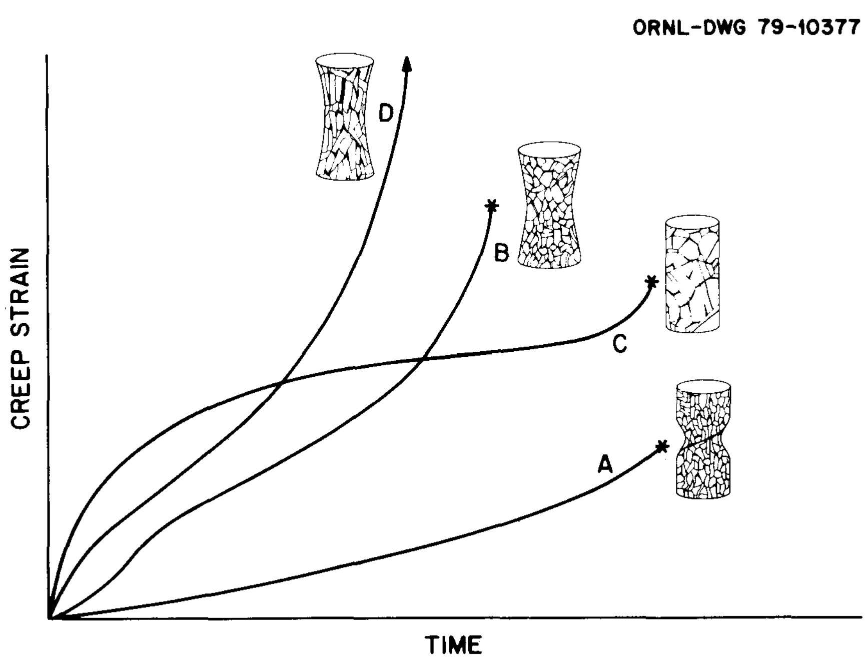

Fig. 23. Typical Creep Curves and Associated Failure Modes for Temperatures in the Range 482 to 871°C (900 to 1600°F).

creep. The apparent secondary creep rate is very low and is typified by curve C in Fig. 23. The $M_{23}C_6$ carbide has probably precipitated and aids the development of a highly creep-resistant substructure (see Figs. 24 and 25).

At 538°C (1000°F) plastic strain and the kinetics of the $M_{23}C_6$ carbide precipitation interact fairly strongly. The high loading strains associated with high stresses cause grain boundary and matrix carbides to form and grow rapidly, often in the walls of the cellular substructure. However, the particles do not prevent sliding at high stress, and wedge cracks form quickly — even in a tensile test. At high stress the creep curves have the tertiary creep character, indicating that the creep-rupture process is dominated by the recovery of the structure produced by the rapid initial straining. Plastic blunting of wedge cracks occurs, and shear between cracks produces the final rupture. However, at intermediate stress the loading strains are smaller, and carbide precipitation is slower. The dislocation densities in the matrix are lower, and cells are absent. The carbide precipitates on grain boundary dislocations and along dislocations in the matrix. We would surmise that the carbide would promote the development of a creep-resistant substructure with high friction stress and low effective stress. The data in Fig. 9 confirm this.

Creep curves at 566 and 593°C (1050 and 1100°F) are essentially the same, as discussed above. That is, very high stresses produce tertiary or sigmoidal creep curves and intermediate stresses produce curves with large primary stages. The specimens with tertiary and sigmoidal curves exhibit cellular structures. This implies that dynamic and thermal recovery are active in the matrix. The specimens having creep curves with large primary stages all show substructures with a high density of tangles dislocations in a network stabilized by a fine $M_{23}C_6$ carbide precipitate. This implies a strong matrix with minimal recovery. Carbide particles are nearly always in the grain boundaries, and the failures are nearly always intergranular. The presence of wedge cracks is a sure sign that grain boundaries have slid somewhat. The strong matrix apparently cannot accommodate the stresses set up by the sliding process, and triple point cracking occurs. About every third grain has a crack on a facet,

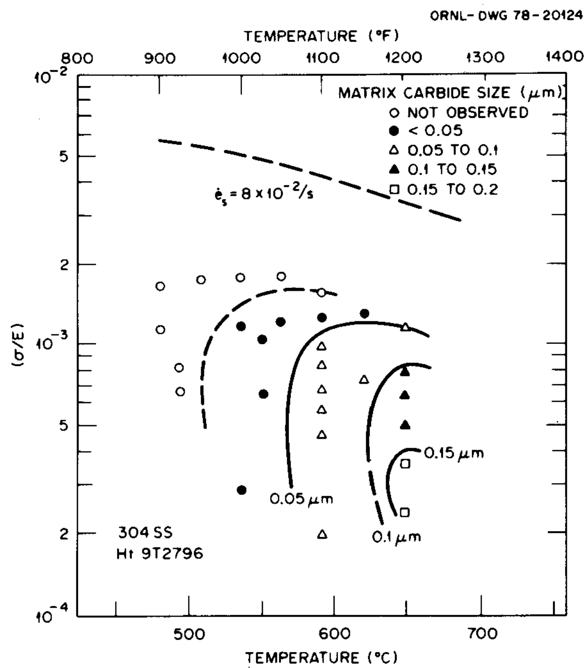

Fig. 24. Matrix Carbide Map to 36 Ms (10,000 h).

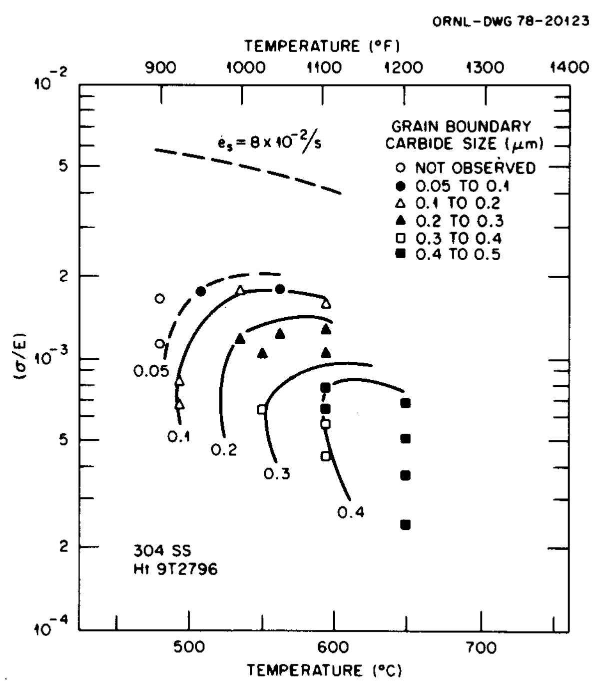

Fig. 25. Grain Boundary Carbide Map to 36 Ms (10,000 h).

and the cracking could possibly relieve the stresses on several nearby grains. Therefore, the loss in creep ductility with decreasing stress could be tied to the inability of the matrix to "recover" or flow plastically between the wedge cracks. The cracks continue to grow and to link, producing a low ductility failure. The grain boundary carbide's exact role is unknown. Certainly, denuding of carbon and chromium from the matrix near the grain boundary could produce adverse effects. On the other hand, this denuding should suppress the dislocation precipitate hardening near grain boundary triple points and should permit the sliding strains to be accommodated by plastic strain in the matrix. Thus denuding might not be deleterious. Sikka[23] and Hammond[30] have a contrasting viewpoint. They have examined the ductility minimum for several alloys and have concluded that the rapid "dynamic recovery" occurring in regions near the grain boundary promotes both grain boundary sliding and development of wedge cracks. Since the matrix away from the boundary is strong and deforms very little, the strain concentration is very local and promotes low overall ductility.

It is interesting to speculate why the rupture life can be described in terms of the fourth power of the effective stress. This equation is not consistent with deformation models for the grain boundary sliding, and this might lead us to conclude that the rupture life and strain are controlled by the matrix deformation parameters, even though the failure initiation sites are wedge cracks produced by sliding. The activation energy data at temperatures up to 566°C (1050°F) could be consistent with a matrix deformation controlled process. However, the activation energy averaged over the temperature range 510 to 816°C (950 to 1500°F) is rather low, which is very puzzling. The activation energy of 199 kJ/mol is very similar to the energy of dislocation "pipe" diffusion (190 kJ/mol).

Morris and Harries[26] found that dislocation pipe diffusion was insignificant in type 316 stainless steel. Frost and Ashby[31] also reject the significance of this mechanism in type 304 stainless steel. Our calculations show that dislocation pipe diffusion, D_D, could be significant relative to volume diffusion, D_v. Frost and Ashby describe the dislocation pipe diffusion coefficient, D_D, as

$$D_D = D_c f_c \ , \tag{16}$$

where D_c is the core diffusion coefficient, and f_c is the fraction of atom sites associated with dislocation cores. They suggest that

$$f_c = a_c \ \rho \ , \tag{17}$$

where a_c is the cross-sectional area of the dislocation core, and ρ is the dislocation line density. They take a_c to be about $5b^2$, where b is burgers vector. They also assume that D_c is about equal to the grain boundary diffusion coefficient. Using the parameter values provided by Frost and Ashby and values for ρ in the range 10^{13} to 10^{14} lines/m^2, we found that D_D was greater than D_v over the temperature range of our data (482 to 871°C). Thus, core diffusion in the region of the propagating wedge cracks could be a possible contributor to the rupture mechanism.

The activation energy (199 kJ/mol) is only 20% higher than the activation energy for grain boundary diffusion (167 kJ/mol). This similarity leads us again to the grain boundaries and the role of $M_{23}C_6$ carbide in intergranular cracking. We feel that at high stresses grain boundaries slide fairly quickly. However, the carbide precipitates on grain boundaries even faster and particles are present before loading. At high stresses and short times failure should seemingly not differ from that at lower temperatures and long times. However, at intermediate stresses grain boundary sliding is slowed. The carbides become fairly large and could act as sites for microvoid formation. Possibly, the grain boundary void growth rate around the particle is controlled by a process that depends on grain boundary diffusion. This would explain the low activation energy. The wedge crack that starts at a triple point could grow by microvoids linking. The size and spacing of the grain boundary carbide particles becomes a critical factor in this process, as discussed recently by Morris and Harries[26] and Raj and Ashby.[32] Analysis of the data based on a model developed recently by Raj and Ashby[32,33] would be valuable since they suggest that the rupture life for constant strain rate should go through a minimum at a temperature around half the melting point.

At temperatures above 649°C (1200°F) the material behavior is more-or-less classical, and the schematic curve D in Fig. 23 is typical of the data trend. Stresses are generally low, and the recovery rates are very high. Subgrains form (Fig. 22) and the carbide particles are large and blocky (Figs. 24 and 25). The recovery is rapid enough to delay the buildup of stresses, which promote wedge cracking at triple points. Fairly large strains are accumulated, and the rupture strains are relatively independent of the stress level. The stress exponent and activation energy for creep are consistent with a dislocation creep model controlled by volume diffusion.

All our data were obtained from tests on unstabilized material. Aging significantly influences the creep behavior. Garofalo,[34] Sikka,[23] Barnby,[35] and others[36] have shown that prior aging greatly improves the creep ductility. We have observed similar effects, and more studies on the subject have been undertaken. We will examine aging effects in a subsequent report when we deal with creep-rupture under varying stresses and temperatures.

CONCLUSIONS

1. The rupture life for type 304 stainless steel can be correlated with engineering stress, S, by a power law. The stress exponent, n, varies with temperature and changes rapidly in the temperature range 593 to 649°C (1150 to 1200°F). The activation energy exceeds that for volume diffusion at high temperatures and is very low at low temperatures.

2. The rupture life can be correlated with modulus-compensated true stress (σ/E) by a power law. The stress exponent, n', varies less with temperature than n but still influences the apparent activation energy, Q. When n varies Q is not unique. The correlation also tends to underpredict long-time low-stress rupture life.

3. The rupture life can be correlated with a modulus-compensated effective stress (σ^*/E) that represents the difference between the applied true stress and a "friction stress," which is temperature dependent. A power law may be used with the stress exponent equal to -4. The activation

energy changes with temperature. When averaged over the 510 to 816°C range the energy is close to 199 kJ/mol (47.6 kcal/mol).

4. The time to tertiary creep, t_3, is proportional to the rupture life, t_R, at most temperatures. In the temperature range 593 to 649°C (1100 to 1200°F) a period exists in which the tertiary creep life is much shorter than expected. The ratio t_3/t_R varies with temperature.

5. The true rupture strain, ε_R, strongly depends on stress and temperature below 649°C (1200°F). At low temperatures ε_R can be related linearly to σ/E. At high temperatures ε_R is relatively constant.

6. The true rupture strain, ε_R, is linearly related to the effective stress for temperatures in the range 482 to 649°C (900 to 1200°F).

7. The true strain at the tertiary limit, ε_3, can be related to the true fracture strain, ε_R, by means of a power law for temperatures up to 593°C (1100°F).

8. The long-time rupture life at temperatures below 649°C (1200°F) cannot be predicted by the Monkman-Grant correlation between the secondary creep rate, $\dot{e}_s$, and the rupture life. The slope of log t_R vs log $\dot{e}_s$ varies with both the temperature and the secondary creep rate.

9. The metallurgical structure changes substantially with stress, temperature, and time and fairly abruptly between 593 and 649°C (1100 and 1200°F).

ACKNOWLEDGMENTS

The author thanks B. C. Williams, who was responsible for the testing. The report was reviewed by V. B. Baylor, R. Huddleston, and R. L. Klueh. The report was edited by B. G. Ashdown and typed by the Publications Office of the Information Center Complex.

REFERENCES

1. J. M. Corum and W. B. Wright, Eds., *Pressure Vessel and Piping: Verification and Qualification of Inelastic Analysis Computer Programs*, American Society of Mechanical Engineers, New York, 1975.

2. M. F. Ashby, *Fracture-Mechanism Maps*, CUED/C/MATS/TR.34, Cambridge University Engineering Department, Cambridge, United Kingdom (undated).
3. H. E. McCoy, Jr. and R. D. Waddell, Jr., "Mechanical Properties of Several Products from a Single Heat of Type 304 Stainless Steel," *J. Eng. Mater. Technol.* 97: 343–49 (1974).
4. R. W. Swindeman, W. J. McAfee, and V. K. Sikka, "Product Form Variability in the Mechanical Behavior of Type 304 Stainless Steel at Room Temperature and 593°C (1100°F)," pp. 41–64 in *Reproducibility and Accuracy of Mechanical Tests, Spec. Tech. Publ. 626*, American Society for Testing and Materials, Philadelphia, 1977.
5. H. E. McCoy, Jr., *Interim Report of Tensile and Creep Data for Type 304 Stainless Steel Plate (Reference Heat 9T2796, 2-in. Thick)*, ORNL/TM-4627 (October 1974).
6. V. K. Sikka, *Long-Term Creep Tests After 30,000 hr on Reference Heat (9T2796) of Type 304 Stainless Steel — Interim Report*, ORNL/TM-6269 (August 1978).
7. C. C. Schultz and W. E. Leyda, *Creep Failure Under Uniaxial and Multiaxial Stress Conditions*, R&D Report LR:79:42;3-01:4, Babcock and Wilcox Company Research Center, Alliance, Ohio (August 1978).
8. S. Y. Zamrik, *Study of Effect of Biaxiality in Creep-Fatigue at Elevated Temperatures, Annual Progress Report*, ORNL-Sub-3649-1 (June 1971).
9. D. L. Herrod and M. J. Manjoine, "Stress-Controlled Creep-Fatigue Tests on 304 Stainless Steel in Air and Vacuum," pp. 87–100 in *1976 ASME-MPC Symposium on Creep-Fatigue Interaction*, MPC-3, R. M. Curran, Ed., American Society of Mechanical Engineers, New York, 1976.
10. O. K. Chopra and K. Natesan, "Interpretation of High-Temperature Creep on Type 304 Stainless Steel," *Metall. Trans.* 8A: 633–38 (1977).
11. Personal Communication, D. Voorhees, Materials Technology Corporation, Ann Arbor, Michigan, ongoing.
12. R. W. Swindeman and C. E. Pugh, *Creep Studies on Type 304 Stainless Steel (Heat 8043813) Under Constant and Varying Loads*, ORNL/TM-4427 (June 1974).
13. V. S. Ivanova, "Creep Ductility Criterion for Metals," *Zavod. Lab.* 21: 212–16 (1955). Butcher Translation No. 4210.

14. M. K. Booker, C. R. Brinkman, and V. K. Sikka, "Correlation and Extrapolation of Creep Ductility Data for Four Elevated-Temperature Structural Materials," pp. 108–45 in *Structural Materials for Service at Elevated Temperatures in Nuclear Power Generation*, MPC-1, A. O. Schaefer, Ed., American Society of Mechanical Engineers, New York, 1975.

15. W. E. Leyda and J. P. Rowe, "A Study of the Time for Departure from Secondary Creep for Eighteen Steels," ASM Technical Report P-6.1, American Society for Metals, Metals Park, Ohio, 1969.

16. F. R. Larson and J. Miller, "A Time-Temperature Relationship for Rupture and Creep Stress," *Trans. ASME* 74: 765–71 (1952).

17. R. L. Orr, O. D. Sherby, and J. E. Dorn, "Correlations of Rupture Data for Metals at Elevated Temperatures," *Trans. Am. Soc. Met.* 46: 113–28 (1954).

18. J. P. Poirier, "Is Power-Law Creep Diffusion Controlled?" *Acta Metall.* 26: 629–37 (1978).

19. R. W. Swindeman, *Correlation of Rupture-Life Creep Rate-Microstructure for Type 304 Stainless Steel Heat 9T2796*, ORNL-5523 (June 1979).

20. C. R. Barrett, A. J. Ardell, and O. D. Sherby, "Influence of Modulus on the Temperature Dependence of the Activation Energy for Creep at High Temperature," *Trans. Metall. Soc. AIME* 320: 200–04 (1964).

21. K. R. Williams and B. Wilshire, "On the Stress and Temperature-Dependence of Creep of Nimonic 80A," *Met. Sci. J.* 7: 176–79 (1973).

22. P. L. Threadgill and B. Wilshire, "Mechanisms of Transient and Steady-State Creep in a γ'-Hardened Austenitic Steel," pp. 8–14, *Creep Strength in Steel and High-Temperature Alloys*, The Metals Society, London, 1974.

23. V. K. Sikka, *Elevated-Temperature Ductility of Types 304 and 316 Stainless Steel*, ORNL/TM-6608 (December 1978).

24. G. V. Smith, Ed., *Characterization of Materials for Service at Elevated-Temperatures MPC-7*, American Society of Mechanical Engineers, New York, 1978.

25. F. C. Monkman and N. J. Grant, "An Empirical Relationship Between Rupture Life and Minimum Creep Rate in Creep-Rupture Tests," *Proc. Am. Soc. Test Mater.* 56: 593–605 (1956).

26. D. G. Morris and D. R. Harries, "Creep and Rupture in Type 316 Stainless Steel at Temperatures Between 525 and 900°C," *Met. Sci. J.* 12: 525–49 (1978).

27. C. N. Ahlquist and W. D. Nix, "A Technique for Measuring Mean Internal Stress During High Temperature Creep," *Scr. Metall.* 3: 679–81 (1969).

28. C. F. Étiènne, W. Dortland, and H. B. Zeedijik, "On the Capability of Austenitic Stainless Steel to Withstand Cyclic Deformation During Service at Elevated Temperature," pp. 225.1–.9 in *Creep and Fatigue in Elevated Temperature Applications* 1, Institute of Mechanical Engineers, London, 1975.

29. T. Shinoda, T. Matsuo, and R. Tanaka, "Method for Improving the Creep Strength in Austenitic Heat-Resisting Steel," pp. 175.1–.9 in *Creep and Fatigue in Elevated Temperature Applications* 1, Institute of Mechanical Engineers, London, 1975.

30. J. P. Hammond, "Ductility Minimum and Its Reversal with Prolonged Aging in Cobalt- and Nickel-Base Superalloys," pp. 63–77 in *Ductility and Toughness Considerations in Elevated Temperature Service*, MPC-8, G. V. Smith, Ed., The American Society of Mechanical Engineers, New York, 1978.

31. H. J. Frost and M. F. Ashby, "Deformation-Mechanism Maps for Pure Iron, Two Austenitic Stainless Steels, and a Low Alloy Ferritic Steel," pp. 27–65 in *Fundamental Aspects of Structural Alloy Design*, R. I. Jaffee and B. A. Wilcox, Eds., Plenum Press, New York, 1977.

32. R. Raj and M. F. Ashby, "Intergranular Fracture at Elevated Temperature," *Acta. Metall.* 23: 653–70 (1975).

33. R. Raj and M. F. Ashby, "Grain Boundary Sliding, and the Effects of Particles on Its Rate," *Metall. Trans.* 3: 1937–42 (1972).

34. F. Garofalo, *Fundamentals of Creep and Creep-Rupture in Metals*, MacMillan Company, New York, 1965.

35. J. T. Barnby, "Effect of Strain Aging on Creep of an AISI 316 Austenitic Stainless Steel," *J. Iron Steel Inst. London* 204: 23–27 (1966).

36. R. W. Swindeman, "Effect of Some Thermomechanical Variables on Plastic Flow and Creep-Rupture of Type 304 Stainless Steel at 593°C," pp. 163–77 in *Effects of Melting and Processing Variables on the Mechanical Properties of Steel*, MPC-6, G. V. Smith, Ed., The American Society of Mechanical Engineers, New York, 1977.

APPENDIX A

Table A1. Summary of Creep Rupture Data

Specimen No.	Engineering Stress (MPa)	Modulus-Compensated True Stress	Time, ks		Status[a]	True Strain, %	
			To Tertiary	In Test		At Tertiary	At Rupture
			482°C				
289	379	306×10^{-6}	(1620)	2405	R	25	42
172	344	269×10^{-6}	(2430)	3186	R	19	26
288	310	224×10^{-6}		13036	R	14	30
	248			>54000	I		
			510°C				
338	372	304×10^{-6}		284	R	25	56
312	344	270×10^{-6}		439	R	20	43
321	310	234×10^{-6}	504	968	R	17	33
296	276	200×10^{-6}	1080	2358	R	13	26
324	241	170×10^{-6}	12240	12639	R	11	22.4
360	172	125×10^{-6}	>80000	>80000	I		
			538°C				
119	344	281×10^{-6}		76	R	22	56
6	310	239×10^{-6}		216	R	17	33
8	276	207×10^{-6}	(468)	587	R	13	25
168	276	205×10^{-6}	(396)	504	R	13	37
9	241	175×10^{-6}	1836	2142	R		
251	241	176×10^{-6}	1242	1260	R	13	33
129	207	146×10^{-6}	7988	7988	R	9	16
	184		>23040	23040	D		
78	172	118×10^{-6}	41540	41540	D		
			566°C				
326	310	250×10^{-6}		36	R	18	39
325	271	210×10^{-6}	104	137	R	17	26
270	241	179×10^{-6}	324	410	R	12	16
294	207	151×10^{-6}	1296	1512	R	11	21
320	172	121×10^{-6}	6228	7394	R	7	11
			593°C				
120	276	220×10^{-6}	17	18	R	14	40
163	276	222×10^{-6}		21	R	15	37
4	241	186×10^{-6}	72	90	R	16	45
86	241	182×10^{-6}	86	108	R	13	31
5	207	154×10^{-6}	288	400	R		
166	207	154×10^{-6}	252	356	R	12	30
43	172	124×10^{-6}	1404	2228	R		20
155	172	125×10^{-6}	1260	1991	R	8	20
54	172	125×10^{-6}	1116	1451	D		
7	172	125×10^{-6}	1008	1584	R		
149	172	125×10^{-6}		2329	R		21
150	172	125×10^{-6}		2495	R	8.9	20
154	172	125×10^{-6}	1440	2128	R		18
159	172	125×10^{-6}		2387	R		24
355	172	125×10^{-6}	1224	1818	R		
32	155	110×10^{-6}	1980	3161	R	6.3	12
162	155	110×10^{-6}	2232	4489	R	5.9	19
239	155	110×10^{-6}	2592	3827	R	6.3	14
258	146	103×10^{-6}	2772	4428	R	5.8	10.4
58	138	98×10^{-6}	16920	18216	D	7.1	9.6
	126	87×10^{-6}	>39600	39600	D		
213	121	84×10^{-6}	46080	55800	R	4.4	8.2
			621°C				
262	207	161×10^{-6}	50	76	R	14	29
263	172	128×10^{-6}	292	428	R	11	22
276	138	98.4×10^{-6}	936	2340	R	5.2	20
	121				R		
266	103	73.6×10^{-6}	16524	16542	R	6.8	17.5
	86		>36000	>36000	I		

Table A1 (Continued)

Specimen No.	Engineering Stress (MPa)	Modulus-Compensated True Stress	Time, ks: To Tertiary	Time, ks: In Test	Status[a]	True Strain, %: At Tertiary	True Strain, %: At Rupture
			649°C				
121	207	164×10^{-6}	7.6	10	R	18	43
167	207	167×10^{-6}	12	16	R		46
1	172	133×10^{-6}	65	101	R	13	36
171	172	136×10^{-6}	47	68	R	15	42
122	155	119×10^{-6}	97	144	R	11	36
210	155	119×10^{-6}	115	194	R	11	30
2	138	103×10^{-6}	180	400	R	7.0	34
85	121	90×10^{-6}	252	900	R	5.3	36
157	121	89.7×10^{-6}	299	1037	R	5.1	36
3	103	75.9×10^{-6}	540	2628	R		
260	95	69.2×10^{-6}	864	3791	R	3.0	22
87	86	64.6×10^{-6}	10800	14256	R	12	84
247	86	64×10^{-6}	7992	4000	D	12	>14
144	69	50×10^{-6}	29635	29635	D	4.7	>6
			704°C				
298	172	145×10^{-6}	2.9	5.8	R	6.4	42
123	138	113×10^{-6}	16	31	R	4.7	54
124	121	98.3×10^{-6}	61	83	R	16	53
299	117	92.9×10^{-6}	30	79	R		34
27	103	80.2×10^{-6}	72	169	R		
297	103	82.8×10^{-6}	94	252	R	6.6	36
T248	95	73.7×10^{-6}	180	299	R	11	33
102	86	70.3×10^{-6}	468	878	R	14	54
295	86	68.2×10^{-6}	324	612	R	11	30
T12	77	63×10^{-6}	1350	2027	R	18	49
160	69	56.5×10^{-6}	2340	3697	R	18	46
391	60	51.9×10^{-6}	7560	11160	R	20	54
255	52	38.6×10^{-6}	6156	(8266)	R		13
			760°C				
109	138	120×10^{-6}	1.8	2.7	R	20	48
110	121	104×10^{-6}	4.7	7.6	R	17	45
118	103	87.4×10^{-6}	9	19	R	13	46
T245	86	70.8×10^{-6}	31	58	R	12	45
83	86	72.3×10^{-6}	43	72	R	15	46
250	69	56×10^{-6}	151	220	R	13	31
30	69	55.3×10^{-6}	108	166	R		
211	59	49×10^{-6}	432	706	R	16	48
84	52	44.7×10^{-6}	1800	2512	R	19	49
			816°C				
111	86	75.2×10^{-6}	4.3	7.6	R	16	58
81	69	59.9×10^{-6}	18	30	R	17	29
80	52	45.2×10^{-6}	227	281	R	22	51
214	34	30.2×10^{-6}	1908	2632	R	28	36
			871°C				
	51.7	55×10^{-6}	25	53	R	53	70
327	34	34×10^{-6}	263	493	R	18	45
392	27.6	27.6×10^{-6}	1260	1300	R	14	37

[a]R — Ruptured, I — in test, and D — discontinued.

APPENDIX B

Table B1. Elastic Modulus Data for Type 304 Stainless Steel

Temperature		Modulus	
(°C)	(°F)	(GPa)	(psi)
25	77[a]	195	28.3×10^6
93	200	191	27.7×10^6
204	400	183	26.6×10^6
316	600	175	25.4×10^6
427	800	166	24.1×10^6
482	900	161	23.3×10^6
510	950	158	22.9×10^6
538	1000	155	22.5×10^6
566	1050	152	22.1×10^6
593	1100	150	21.7×10^6
621	1150	147	21.3×10^6
649	1200	144	20.9×10^6
704	1300	139	20.1×10^6
760	1400	132	19.2×10^6
816	1500	126	18.3×10^6

[a]Room temperature.

APPENDIX C

ORNL-DWG 78-20121

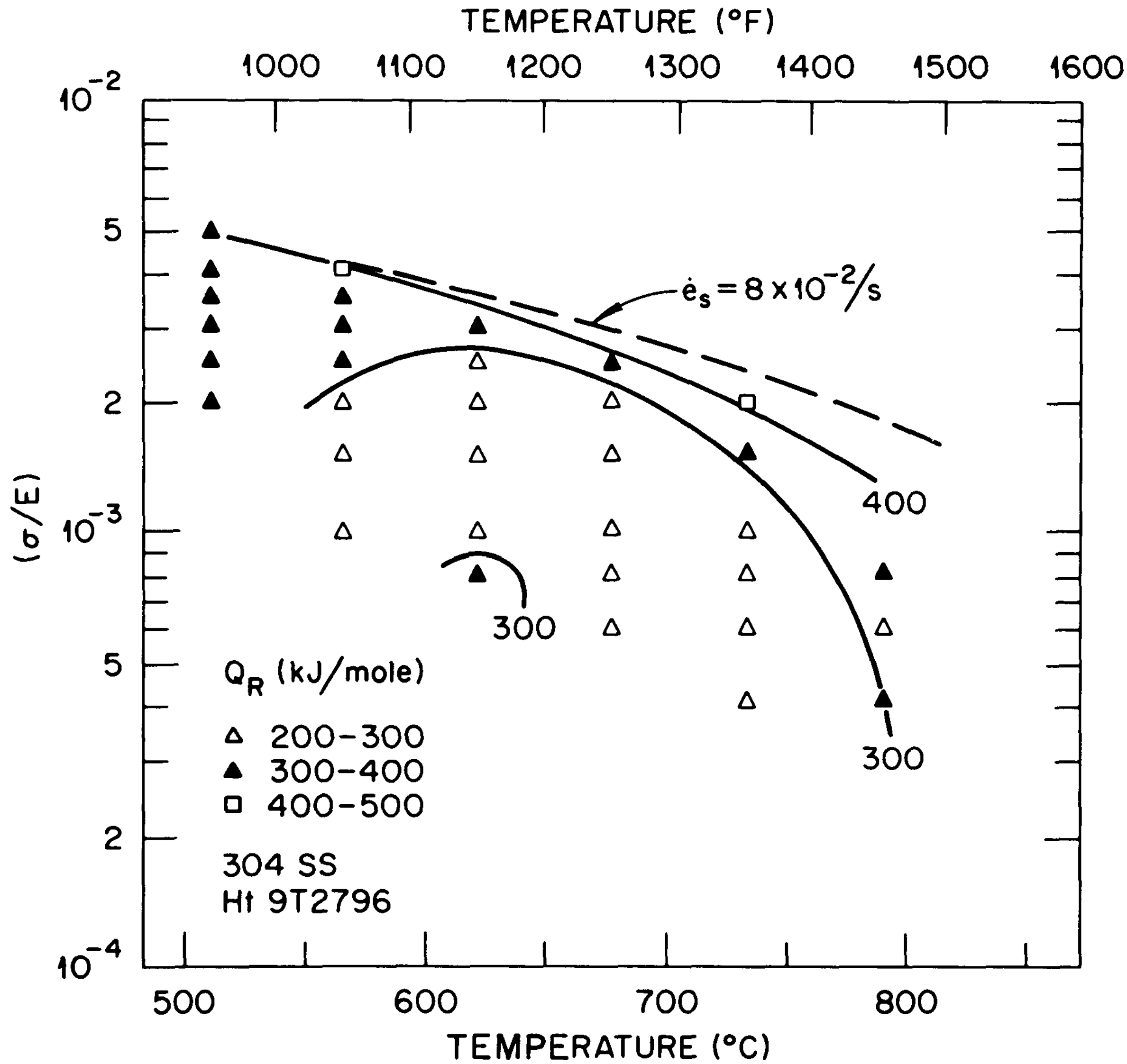

Fig. C1. Variation of the Activation Energy for Rupture with σ/E and T.

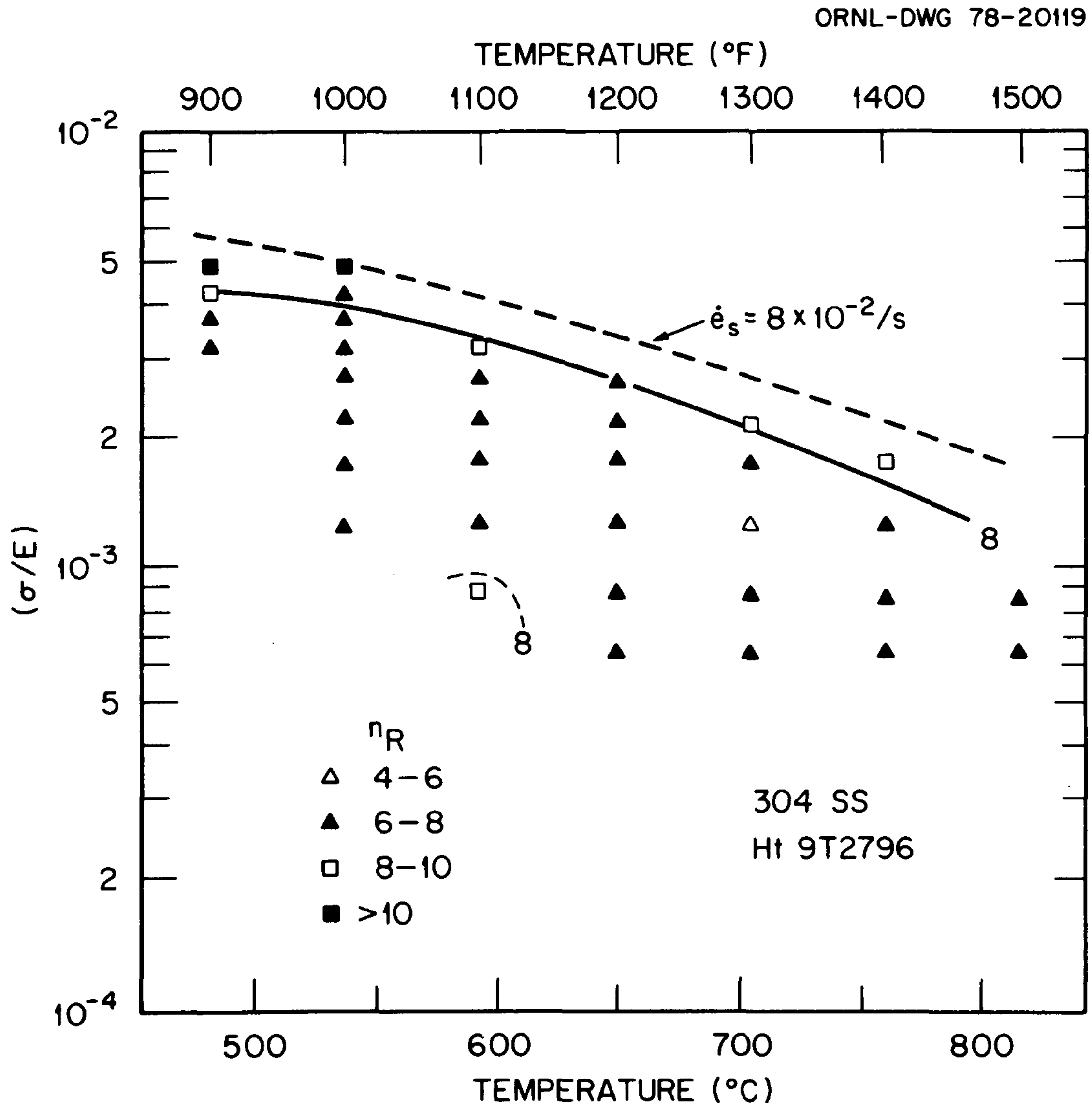

Fig. C2. Variation of the Stress Exponent for Rupture with σ/E and T.

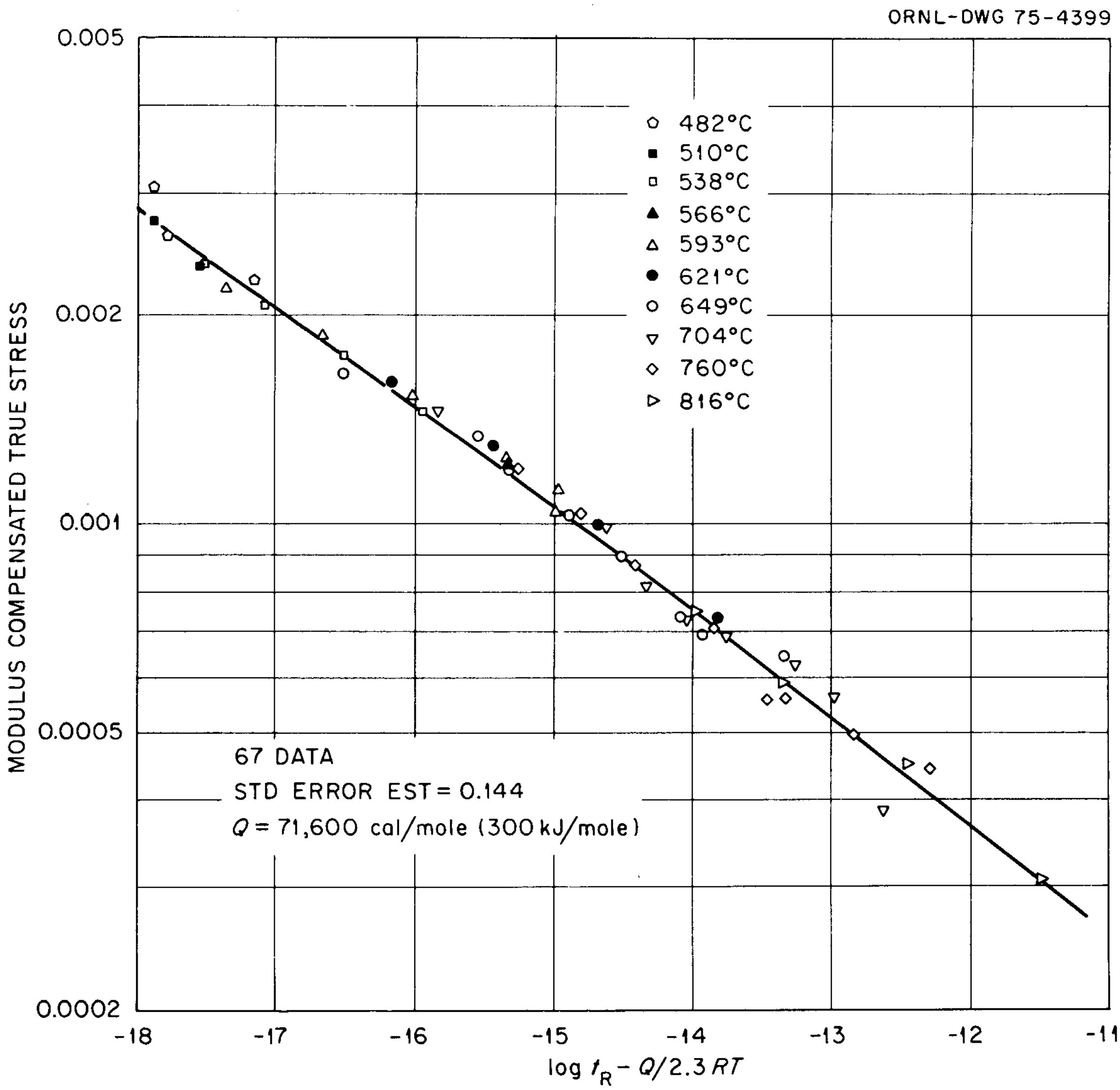

Fig. C3. Plot of Creep-Rupture Data to the Barrett-Ardell-Sherby Parameter.

Blank Page

ORNL-5565
Distribution
Category UC-79b, -h, -k

INTERNAL DISTRIBUTION

1–2. Central Research Library
3. Document Reference Section
4–5. Laboratory Records Department
6. Laboratory Records, ORNL R.C.
7. ORNL Patent Section
8. J. J. Blass
9. M. K. Booker
10. C. R. Brinkman
11. J. A. Clinard
12–13. J. M. Corum
14. G. M. Goodwin
15. W. L. Greenstreet
16. R. F. Hibbs
17–19. M. R. Hill
20. R. L. Huddleston
21. R. L. Klueh
22. K. C. Liu
23. W. J. McAfee
24. H. E. McCoy
25. J. W. McEnerney
26. C. E. Pugh
27. V. K. Sikka
28. G. M. Slaughter
29. J. O. Stiegler
30–49. R. W. Swindeman
50. G. T. Yahr
51. R. W. Balluffi (Consultant)
52. A. L. Bement, Jr. (Consultant)
53. J. F. Harvey (Consultant)
54. W. R. Hibbard, Jr. (Consultant)
55. E. H. Kottcamp, Jr. (Consultant)
56. M. J. Mayfield (Consultant)
57. E. T. Onat (Consultant)
58. J. T. Stringer (Consultant)

Subcontractors

59. H. Armen, Jr., Grumman Aeorspace Corp., Bethpage, NY 11714
60. J. M. Chern, Foster-Wheeler Energy Corp., 110 S. Orange Avenue, Livingston, NJ 07039
61. C. E. Jaske, Battelle-Columbus Laboratories, 505 King Avenue, Columbus, OH 43201
62. W. J. O'Donnell, O'Donnell and Associates, 5100 Centre Avenue, Pittsburgh, PA 15236
63. S. Y. Zamrik, Pennsylvania State University, University Park, PA 16802

EXTERNAL DISTRIBUTION

64–65. DOE DIVISION OF REACTOR RESEARCH AND TECHNOLOGY, Washington, DC 20545

Director

66. DOE OAK RIDGE OPERATIONS OFFICE, P.O. Box E, Oak Ridge, TN 37830

Assistant Manager, Energy Research and Development

67–275. DOE TECHNICAL INFORMATION CENTER, Office of Information Services, P.O. Box 62, Oak Ridge, TN 37830

For distribution as shown in TID-4500 Distribution Category, UC-79b (Fuels and Materials Engineering Development); UC-79h (Structural Materials Design Engineering); UC-79k (Components).

☆U.S. GOVERNMENT PRINTING OFFICE: 1979-640-079-204